https://doi.org/10.5194/bg-2019-257
Preprint. Discussion started: 8 July 2019


Biogeosciences Discussions

# Decoupling of net community production and particulate organic carbon dynamics in near shore surface ocean waters

Sarah Z. Rosengard[1], Robert W. Izett[1], William J. Burt[2], Nina Schuback[3,4], and Philippe D. Tortell[1,5]

1. Department of Earth, Ocean and Atmospheric Sciences, University of British Columbia, Vancouver, V6T 1Z4, Canada
2. College of Fisheries and Ocean Sciences, University of Alaska Fairbanks, Fairbanks, 99775, USA
3. Swiss Polar Institute, Lausanne, CH-1015, Switzerland
4. École Polytechnique Fédérale de Lausanne, Lausanne, CH-1015, Switzerland
5. Department of Botany, University of British Columbia, Vancouver, V6T 1Z4, Canada

*Correspondence to: Sarah Z. Rosengard (srosengard@eoas.ubc.ca)*

https://doi.org/10.5194/bg-2019-257
Preprint. Discussion started: 8 July 2019


Biogeosciences Discussions Open Access EGU

**Abstract.** We report results from two Lagrangian surveys off the coast of Oregon, using continuous ship-board sensors to estimate mixed layer net community production (NCP) from diel cycles in biological oxygen saturation ($\Delta O_2/Ar$) and optically-derived estimates of particulate organic carbon (POC) and phytoplankton carbon ($C_{ph}$). The first drifter survey, conducted in a nearshore upwelling zone during the development of a microplankton bloom, exhibited significant differences in NCP derived from $\Delta O_2/Ar$ and POC diel cycles, suggesting the presence of large POC losses from the mixed layer. At this site, we utilized the discrepancy between $NCP_{O2/Ar}$ and $NCP_{POC}$, along with additional constraints derived from mixed layer nutrient inventories and surface water excess nitrous oxide ($N_2O$), to estimate particle export, vertical mixing fluxes and DOC production. We estimate that export, vertical mixing and DOC production account for 13-45%, 24-38% and 25-49% of the daily NCP discrepancy, respectively. In contrast, the second drifter survey occurred in more oligotrophic offshore waters, where NCP derived from $\Delta O_2/Ar$ and POC measurements were more closely coupled, suggesting a tighter relationship between production and community respiration. These results support the use of diel POC measurements to accurately estimate NCP in lower productivity waters with limited vertical carbon export. Although diel POC measurements may underestimate NCP in higher productivity waters, our results highlight the potential utility of coupled $O_2$ and optical measurements to estimate the fate of POC in such regions.

## 1 Introduction

Net community production (NCP) represents the balance between water column photosynthesis and community respiration, and sets an upper limit on carbon export from the surface mixed layer. Accurate assessment of NCP is thus critical to understanding trophic balance and the fate of organic carbon in the surface ocean, yet this variable remains challenging to quantify on ecologically-relevant time and space scales. In recent years, automated *in situ* measurements of seawater optical properties have been increasingly used to estimate gross and net primary productivity (GPP and NPP, respectively), and to infer NCP at high temporal resolution (e.g., Graff et al., 2016; Burt et al., 2018). Specifically, a number of authors have exploited the relationship between particulate organic carbon (POC) concentrations and the beam attenuation coefficient ($c_p$) (Siegel et al., 1989; Stramska and Dickey, 1992; Gardner et al., 1993;

https://doi.org/10.5194/bg-2019-257
Preprint. Discussion started: 8 July 2019


Claustre et al., 1999; Gernez et al., 2011) to resolve diel cycles in POC. These diel cycles reflect the accumulation and loss of fixed carbon through photosynthesis and respiration, and can thus be used to infer NCP on daily time-scales. To date, much of this work has focused on low productivity offshore regions, where there is limited particle export and/or POC loss to the dissolved organic carbon (DOC) pool (Claustre et al., 2007; White et al., 2017). These studies have reported good agreement between optically-derived GPP estimates and independent estimates of NPP from $^{14}C$ incubations (White et al., 2017), suggesting a tight coupling between primary productivity and mixed layer POC dynamics over these short time scales.

Another approach to NCP quantification is based on autonomous measurements of surface water dissolved oxygen to argon ratios ($O_2$/Ar). Argon normalization is used to correct for any physically-induced changes in $O_2$ saturation, so that the derived saturation anomaly, $\Delta O_2$/Ar, represents the biologically-induced net $O_2$ production (Kaiser et al., 2005; Tortell, 2005; Cassar et al., 2009). At steady-state, and in the absence of significant lateral advection and vertical mixing, the sea-air flux of excess biologically-produced $O_2$ is equivalent to NCP, providing an indirect measure of carbon export out of the mixed layer. With the development of automated ship-board mass spectrometers, there has been a significant increase in surface water $O_2$/Ar measurements, and these have been used to examine $O_2$/Ar variability resulting from diel cycles of photosynthesis and respiration, and to infer NCP in a variety of oceanic ecosystems (Reuer et al., 2007; Stanley et al., 2010; Tortell et al., 2011, 2014; Hamme et al., 2012; Nicholson et al., 2015; Manning et al., 2017).

Combined measurement of mixed layer POC and $O_2$ dynamics holds the potential to better constrain surface water carbon budgets at high spatial and temporal resolution. In net autotrophic systems, an increase in $\Delta O_2$/Ar reflects the accumulation of excess photosynthetic $O_2$ in the mixed layer, but provides no direct insight into the fate of the resulting organic carbon. In the absence of particle export or DOC production, an increase in $\Delta O_2$/Ar, corrected for air-sea exchange and vertical mixing, should be matched by a parallel increase in POC accumulation measured by optical sensors. By comparison, high POC export or DOC production would act to decouple $\Delta O_2$/Ar from optically-derived POC measurements in the mixed layer.

Previous authors have used simultaneous $O_2$ and particulate $c_p$ measurements on moorings to describe mixed layer $O_2$ and POC dynamics in various marine environments (Stramska and Dickey, 1992; Kinkade et al., 1999; Dickey and Chang, 2002). However, few

https://doi.org/10.5194/bg-2019-257
Preprint. Discussion started: 8 July 2019


78 studies to date have compared estimates of primary productivity from simultaneous
79 measurements at daily time scales. Briggs et al. (2018) and Alkire et al. (2012) were the first to
80 explicitly combine concurrent measurements of $O_2$ and POC from *in situ* autonomous sensors to
81 quantify mixed layer productivity during a ~2-month Lagrangian study of the 2008 North
82 Atlantic spring bloom. Tracking daily changes in mixed layer $O_2$ and POC concentrations, Alkire
83 et al. (2012) constructed a detailed budget of surface ocean organic carbon throughout the course
84 of the bloom, using the difference between $O_2$-based NCP and net POC accumulation to assess
85 the partitioning of NCP into different carbon pools (sinking particles, phytoplankton biomass,
86 and DOC). Building on this work, Briggs et al., (2018) examined the role of respiration, particle
87 export, and DOC production in decoupling $O_2$ and POC dynamics through different bloom
88 stages, demonstrating large differences between GPP estimates derived from these various proxy
89 measurements. To our knowledge, such a detailed examination of $O_2$ and POC dynamics has not
90 been reported for other marine systems.
91 In this study, we present new results from a field study of diel variability in $\Delta O_2/Ar$ and
92 optical properties in two contrasting near-shore regions of the Subarctic North Pacific. Using
93 ship-board automated sensors deployed along a Lagrangian drifter track, we resolved fine-scale
94 temporal patterns in biological oxygen production and POC concentration in a high productivity
95 coastal upwelling zone over the continental slope and lower productivity stratified waters off
96 shore. Extending findings from the 2008 North Atlantic bloom, we derived NCP estimates from
97 $O_2/Ar$ and optically-derived POC measurements in water masses with different trophic status and
98 phytoplankton assemblage composition. Our results demonstrate significant uncoupling between
99 $\Delta O_2/Ar$ and POC in the two systems, with differences between the sites that likely reflect
100 variability in carbon export capacity and DOC production. We discuss the implications of these
101 results for understanding biological carbon cycling in coastal marine waters, and suggest
102 additional approaches to improve the utility of coupled $\Delta O_2/Ar$ and optically-derived organic
103 carbon measurements for assessing the fate of marine primary productivity.
104
105 **2 Methods**
106
107 **2.1 Field site and Lagrangian surveys**
108

https://doi.org/10.5194/bg-2019-257
Preprint. Discussion started: 8 July 2019


Field studies were conducted on board the R/V *Oceanus* in August 2017, during a transect through the Northeast Subarctic Pacific Ocean. Two Lagrangian drifters were deployed off the Oregon coast, allowing us to track diurnal patterns in phytoplankton productivity and particulate organic carbon cycling in two distinct water masses (Fig. 1). Underway temperature and salinity measurements, collected by a Seabird SBE 45 thermosalinograph, as well as satellite (Aqua MODIS) and ship-based chlorophyll-a (Chl-a) observations, were used to guide the specific location and timing of the two drifter deployments. Drifter 1 was deployed on 20 August 2017 (~9:30 PDT), ~40 km from the Oregon coast (44.54° N, 124.58° W), in the vicinity of an upwelling feature detected based on low sea surface temperature, and elevated salinity and [Chl-a]. The drifter, consisting of a beacon, GPS transmitter and 5 m drogue, was recovered at ~18:30 on 23 August 2017 (44.40° N, 124.55° W) for a total deployment of 3 days and 9 hours. Upon recovery, the drogue was missing, implying the potential for some erratic sub-surface drifting (discussed below). Drifter 2 was deployed approximately 200 km from shore (43.75° N, 126.50 °W) in a relatively warm and low salinity water mass, with low Chl-a concentrations. This second drifter was deployed at ~07:45 on 24 August 2017, and was recovered after 2 days and six hours at ~14:00 on 26 August 2017 at 43.80° N, 126.99° W. Because the *Oceanus* lacks a dynamic positioning system, the ship was not always able to perfectly track the drifter locations. To correct for these positional offsets, we discarded any observations obtained when the ship was more than 1.5 km away from the drifter location. This filtered dataset resulted in measurements every ~15 minutes during the two drifter deployments, yielding 325 and 218 quality-controlled underway observations for drifters 1 and 2, respectively.

## 2.2 Underway measurements

Continuous underway measurements of surface seawater optical properties were collected using Seabird ECO-BB3 and ac-s sensors, following the methods outlined in detail by Burt et al. (2018). Water was collected from the ship's seawater supply system with a nominal intake of 5 m depth. Our instrument package includes fully automated data collection, and hourly filtered blanks (0.2µm), which provide measurements of dissolved seawater optical properties used to infer particulate absorption ($a_p$) and beam attenuation ($c_p$) at 82 wavelengths between 400 and ~735 nm, and backscatter ($b_{bp}$) at 470 nm, 532 nm, and 650 nm. The BB-3 and ac-s

https://doi.org/10.5194/bg-2019-257
Preprint. Discussion started: 8 July 2019




measurements were binned into 1-minute intervals. Prior to binning, the absorption and beam attenuation data were first sub-sampled every 50 data acquisition cycles (~12.5 seconds) to enable faster processing time. The optical measurements were accompanied by continuous surface photosynthetically active radiation (PAR) and windspeed data obtained from a Biospherical QSR-220 PAR sensor and Gill WindObserver II ultrasonic wind sensor mounted on the ship's bow, respectively.

Chlorophyll-a (Chl-a) concentrations were derived from the particulate absorption line height at 676 nm ($a_{LH}$) (Roesler and Barnard, 2013). Five-minute match-ups between underway $a_{LH}$ and discrete [Chl-a] measurements from the entire cruise transect (Sect. 2.4) were used to derive a best fit coefficient for the linear relationship between $a_{LH}$ and [Chl-a] ($r^2$=0.87, n= 58, $p<0.01$). Particulate organic carbon (POC) concentrations (µg/L) were derived from particulate beam attenuation at 660 nm ($c_{p,660}$), using the empirical model in Graff et al. (2015). Similarly, phytoplankton organic carbon ($C_{ph}$) concentrations were calculated, using an empirical relationship between particulate backscatter at 470 nm ($b_{bp,470}$) and [$C_{ph}$] in µg/L (Graff et al., 2015). We used a limited set of 5m discrete measurements (n=6) to evaluate the relationship between POC concentrations and $c_p$ at 660nm. As shown in Fig. S1, the POC measurements were significantly correlated to $c_p$ ($r^2$=0.94, $p<0.05$), with a slope and intercept of 443.2 ± 161.5 and 27.7 ± 59.3, respectively. This slope was very similar to that of the Graff et al. algorithm (419.8) although our y-intercept was higher. Notwithstanding the relatively small number of discrete POC samples, and some scatter around the regression line, the similarity of our POC-$c_p$ calibration to that reported by Graff et al. (2015) suggests that our optically-derived POC estimates are relatively robust.

To obtain information on the particle size spectrum, we derived the wavelength-dependent slope of particulate backscatter by fitting the three $b_{bp}$ coefficients (470 nm, 532 nm, 650 nm) to an exponential equation (Stramska et al., 2003; Loisel et al., 2006; Kostadinov et al., 2009). Finally, to assess interference of inorganic minerals on POC, and $C_{ph}$ variability, we calculated the wavelength-specific bulk refractive index ($\eta_p$) from backscatter/total scatter ratios ($\frac{b_{bp}}{c_p - a_p}$) and the wavelength-dependent $c_p$ slope, following the approach of Boss et al. (2001), Twardowski et al. (2001) and Sullivan et al. (2005).

In addition to optical measurements, the seawater biological oxygen saturation anomaly ($\Delta O_2/Ar$) was measured at ~20 second resolution using a membrane inlet mass spectrometer

https://doi.org/10.5194/bg-2019-257
Preprint. Discussion started: 8 July 2019




connected to the ship's seawater intake. The seawater ratio of dissolved $O_2$ and Ar was determined by diverting a continuous flow of water across a dimethylsilicone membrane interfaced with a Hiden Analytical HAL20 triple filter quadropole mass spectrometer. The $O_2$/Ar ratio of air-equilibrated standards ($[O_2/Ar]_{eq}$), incubated at ambient sea surface temperature, was measured every two hours. Values of $\Delta O_2$/Ar were thus calculated as the percent deviation of seawater $O_2$/Ar measurements from the air-equilibrated ratio, using $\Delta O_2/Ar = 100\% * ([O2/Ar]_{meas} / [O_2/Ar]_{eq} - 1)$ (Tortell, 2005; Tortell et al., 2011).

### 2.3 Mixed layer depth

Over the course of both drifter deployments, we conducted regular hydrographic casts (every six to ten hours) to examine depth profiles of seawater hydrography and biogeochemical variables. Temperature, salinity, dissolved $O_2$ concentrations and Chl-a fluorescence profile data from the CTD casts were measured by a Seabird-SBE 38 temperature sensor, Seabird-SBE 4 conductivity sensor, SBE 43 dissolved $O_2$ sensor, and a Seabird ECO fluorometer, respectively, and binned into 1 m intervals. Due to recent upwelling, vertical profiles at the drifter 1 site showed relatively weak density stratification. For this reason, we estimated mixed layer depths ($z_{mld}$) based on visible inflection points in the dissolved [$O_2$], fluorescence and density profiles, assuming that dissolved $O_2$ concentrations and fluorescence are relatively uniform in the mixed layer (Fig. 2a). Within a single CTD cast, mixed layer depths varied by up to 28% across all three profile measurements. The [Chl-a] fluorescence profiles had most well-defined inflection points, and we thus used these data to estimate $z_{mld}$ at all casts. Excluding fluorescence profiles from the first day (Sect. 3.1), and two casts at 6am and midnight on second and third 24-hour intervals, respectively, which displayed an anomalously shallow $z_{mld}$ (< 10 m) and relatively noisy density profiles, an average $z_{mld}$ value (19 ± 2 m) was applied to all subsequent analyses.

In comparison to the drifter 1 site, CTD cast profiles during drifter deployment 2 showed clearer density stratification. We thus computed $z_{mld}$ using a density difference criterion of 0.25 kg/m$^3$ (Thomson et al., 2003; de Boyer Montégut et al., 2004) from median values within the upper-most 4–6 m of the profile. In all CTD casts except one, density difference-based $z_{mld}$ values were within 5 meters of the values derived from the inflection points on density profiles.

https://doi.org/10.5194/bg-2019-257
Preprint. Discussion started: 8 July 2019


Biogeosciences Discussions Open Access EGU

An average $z_{mld}$ value estimated from the density-difference approach (22 ± 5 m) was applied to all subsequent analyses.

**2.4 Discrete samples**

Concentrations of phosphate ($[PO_4^{3-}]$), dissolved silica ($[SiO_2]$), and nitrate and nitrite ($[NO_3^- + NO_2^-]$, were measured in seawater samples collected from daily Niskin bottle casts. Following collection, nutrient samples were filtered through 0.2 µm pore polycarbonate membranes and immediately frozen at -80°C on board the ship. These samples were later stored at -20°C until subsequent colorimetric laboratory analyses (Murphy and Riley, 1962; Riley, 1977) with a Lachat QuikChem 8500 Series 2 Flow Injection Analysis System.

Concentrations of nitrous oxide ($N_2O$) were measured in discrete samples collected in Niskin bottles during both drifter deployments, following methods outlined in (Capelle et al., 2015). These $N_2O$ measurements were used to correct NCP estimates for vertical mixing (see Sect. 2.6), following the approach described by Cassar et al. (2014) and Izett et al. (2018).

Surface (~5 m) discrete seawater samples were collected from Niskin bottles or from the ship's surface seawater intake system for HPLC analysis of Chl-a concentrations and other phytoplankton pigments. Single or duplicate samples were filtered onto 25 mm GF/F filters, flash-frozen in liquid nitrogen, and stored at -80°C until analysis, following the methodology described in (Schuback et al., 2016). Additional samples were collected from the seawater intake for size-fractionated Chl-a analysis (Zeng et al., 2018). These samples were filtered through stacked 47 mm filters (0.2 µm, 2 µm and 20 µm pore size) separated by a mesh spacer. Filtered samples were extracted in 5 mL of 90% acetone at 4°C until analysis within 24–48 hours using a Turner Trilogy Fluorometer on board the ship.

Discrete samples for POC analysis were collected at two depths from several CTD casts. Surface samples were collected at both drifter sites from 5 m depth, while deeper samples were collected at near the base of the euphotic zone (1% PAR), corresponding to 40–60 m at drifter site 1, and 100–120 m at drifter site 2. POC samples (~1–4 L) were filtered through a pre-combusted (450 °C) Whatman GF/F filter (nominal pore size ~ 0.7 µm), and stored at -80°C until laboratory analysis. Prior to analysis, samples were thawed and dried at 50°C overnight, fumigated with concentrated hydrochloric acid for 48 hours, and dried again at 50°C overnight.

https://doi.org/10.5194/bg-2019-257
Preprint. Discussion started: 8 July 2019




232 POC concentrations in samples (and blank combusted filtered treated as described above) were
233 quantified using an *Elementar* vario MICRO cube CHNS analyzer. Blank-corrected discrete
234 POC concentrations were used to validate application of the [POC] model in Graff et al. (2015)
235 to our underway $c_p$ data (Sect. 2.2; Fig. S1).
236
237 **2.5 Net Primary Productivity**
238
239 Daily-integrated net primary productivity (NPP) was calculated in two ways. First,
240 carbon uptake was determined from 24-hour $^{14}C$-incubations with 5 m triplicate seawater
241 samples collected from early morning CTD casts. Measurements were made on two different
242 mornings during drifter deployment 1 and on one morning during drifter deployment 2. The
243 measurements were conducted following the protocol outlined in Hoppe et al. (2017). Depth-
244 integrated NPP was calculated by multiplying the derived 24-hour carbon fixation rate by the
245 average mixed layer depth for the respective drifter period.
246 Second, daily-integrated net primary productivity was also estimated as a product of [$C_{ph}$]
247 values derived from $b_{bp}$, and phytoplankton growth rates according to the carbon-based
248 productivity model (CbPM) (Behrenfeld et al., 2005; Westberry et al., 2008; Graff et al., 2016;
249 Burt et al., 2018). In these calculations, daily-averaged [$C_{ph}$], [Chl-a]/[$C_{ph}$], and mixed layer
250 irradiance ($E_g$) calculated from the MODIS-derived surface PAR matched to drifter location
251 were used to calculate growth rates and NPP every 24 hours. Chlorophyll-a concentrations were
252 derived from absorption line height (Sect. 2.2), [$C_{ph}$] values from $b_{bp}$, and light extinction
253 coefficients ($K_d$) used to calculate $E_g$ from [Chl-a] (Morel et al., 2007). An average mixed layer
254 depth for each drifter period was applied to estimate mixed layer NPP (Sect. 2.3).
255
256 **2.6 Quantification of diurnal cycles and NCP**
257
258 We quantified net community production (NCP) based on the analysis of diel cycles in
259 $\Delta O_2/Ar$ ($NCP_{O2/Ar}$) and POC ($NCP_{POC}$), by examining changes in these quantities over
260 subsequent day and night intervals. In all calculations described below, daily-integrated NCP
261 values were taken as the sum of daytime (D) and nighttime (N) values. Daytime was defined as
262 the period during which PAR levels exceeded 20 µmol quanta $m^{-2}s^{-1}$. The average length of the

https://doi.org/10.5194/bg-2019-257
Preprint. Discussion started: 8 July 2019




day-time period, $t_D$, was 13.6 ± 0.14 hours over the two drifter deployments. Daily NCP values were integrated through the mixed layer using the average $z_{mld}$ for each drifter period, as described in Sect. 2.3.

Quantification of NCP from diurnal cycles in $\Delta O_2/Ar$ requires corrections for gas exchange and, potentially, vertical mixing fluxes. For these calculations, we first computed the rate of change in $\Delta O_2/Ar$ ($dO_{2Bio}/dt$) using linear regression analysis within successive daytime or nighttime intervals. We then derived estimates for the air-sea gas exchange ($J_{ex}$) and vertical mixing fluxes ($F_{mix}$) to isolate the NCP contribution to observed $\Delta O_2/Ar$ changes (Izett et al., 2018; Tortell et al., 2014). Net $O_2$ production rates were converted into carbon units using a photosynthetic quotient for new production (PQ) of 1.4 (Laws, 1991).

$$NCP_{O2/Ar} = \frac{t_d NCP_D + t_N NCP_N}{PQ} \quad (1)$$

$$NCP_{D\ or\ N} = z_{mld} \frac{dO_{2bio}}{dt} + J_{ex} + F_{mix} \quad (2)$$

$$O_{2bio} = \frac{\Delta O_2}{Ar} \frac{1}{100\%} O_{2eq} \quad (3)$$

$$J_{ex} = k_{o2} O_{2bio} \quad (4)$$

$$F_{mix\ (\frac{O2}{Ar})} = k_{mix} \frac{dO_{2bio}}{dz} \quad (5)$$

$$k_{mix} = k_{N2O} N2O_{bio} (\frac{dN2O_{bio}}{dz})^{-1} \quad (6)$$

$$N_2O_{bio} = N2O_{meas} - N2O_{eq} - N2O_{thermal} \quad (7)$$

Equilibrium concentrations of $O_2$ and $N_2O$ ($[O_2]_{eq}$ and $[N_2O]_{eq}$) were calculated using the salinity and temperature-dependent equations of Garcia and Gordon (1992) and Weiss and Price (1980), respectively, and sea surface temperature and salinity from the ship's thermosalinograph. Estimates of surface excess $N_2O$ saturation, $[N_2O]_{bio}$, included a heat flux correction to account

https://doi.org/10.5194/bg-2019-257
Preprint. Discussion started: 8 July 2019




for solubility changes ( Keeling and Shertz, 1992; Jin et al., 2007; Izett et al., 2018). Non-weighted piston velocities ($k_{O2}$ and $k_{N2O}$) were calculated using the diffusive air sea gas flux and Schmidt number parameterizations of Wanninkhof (2014) and Raymond et al. (2012), and ship-based wind speed data 10 m above the sea surface. Daytime and nighttime estimates for the gas exchange term, $J_{ex}$, were calculated using day/night average $[O_2]_{eq}$, $\Delta O_2/Ar$, and $k_{O2}$ values. Daytime and nighttime $F_{mix}$ was calculated using $[N_2O]_{bio}$ values averaged over the entire drifter deployment, daytime/nighttime average $k_{N2O}$ values, and a vertical gradient term derived from all of the $O_2$ and $N_2O$ profile data for the cruise. At drifter site 2, vertical mixing was considered negligible in the absence of $N_2O$ super-saturation in surface waters.

We used the approach of (Claustre et al., 2007) to calculate daily-integrated NCP from daytime and nighttime changes in POC (dPOC/dt), calculated from linear regressions of POC concentrations against time through day and night intervals.

$$NCP_{POC} = z_{mld}\left[t_D\left(\frac{dPOC}{dt}\right)_D + t_N\left(\frac{dPOC}{dt}\right)_N\right] + F_{mix\,(POC)} \quad (8)$$

Because of significant upwelling at drifter site 1 (Fig. 1), entrainment of particle-poor seawater from below the mixed layer into the surface could dilute the $c_p$ signal used to derive POC concentrations (Stramska and Dickey, 1994). Applying the constant $k_{mix}$ derived from Eq. (6), the average daily dilution effect on mixed layer POC concentrations through drifter period 1 was additionally quantified and accounted for, as such:

$$F_{mix\,(POC)} = k_{mix}\frac{dPOC}{dz} \quad (9)$$

The term d[POC]/dz represents the vertical gradient in [POC], derived from average POC concentrations measured in CTD samples at 5 m and average [POC] measured near the base of the euphotic zone, below the mixed layer (40–60 m) (Sect. 2.4). At drifter site 2, $F_{mix,POC}$ was assumed negligible since the derived vertical mixing term was close to zero.

In total, three $NCP_{O2/Ar}$ and $NCP_{POC}$ values were calculated during the drifter 1 deployment, from the three pairs of consecutive day and night intervals, starting with the first night interval and ending with the last day interval. We excluded the first day-time interval from

https://doi.org/10.5194/bg-2019-257
Preprint. Discussion started: 8 July 2019




our calculations, due to the erratic salinity values observed during the first day of this drifter deployment (Sect. 3.1; Fig. S2). Because the drifter period was terminated prior to sunset, the last day interval was 1.6 hours shorter than the average daytime duration. For the second drifter deployment, two $NCP_{O2/Ar}$ and $NCP_{POC}$ values were calculated from consecutive day and night intervals, starting with the first daytime interval and ending with the last nighttime interval. The initiation of the drifter period occurred after sunrise, so the first day interval was 1.1 hours shorter than the average daytime duration.

We also used a similar approach to estimate a phytoplankton-specific net accumulation rate, substituting $C_{ph}$ for POC in Eq. (8). Because no vertical phytoplankton carbon concentration profiles were measured, net $C_{ph}$ accumulation rates were not corrected for mixing of deep water at drifter site 1.

**2.7 Error analysis**

Errors for all estimates of net primary productivity (CbPM-NPP, $^{14}$C-NPP), net community production ($NCP_{O2/Ar}$, $NCP_{POC}$) and $C_{ph}$ accumulation were propagated from uncertainties associated with mixed layer depth, day/night duration, variable averages, linear regressions (Eqs. (1), (8)), and underway measurements (Burt et al., 2018; Izett et al., 2018). The uncertainty in $z_{mld}$ was 2 m for drifter site 1 and 5 m for drifter site 2 (Sect. 2.3). Uncertainties in $t_D$ and $t_N$ were the standard deviations of all day or night lengths measured during both drifter periods (0.14 and 0.10 hours, respectively). Mean relative errors of [Chl-a] and [$C_{ph}$] from Burt et al. (2018), and mean relative standard deviations in MODIS-derived daily surface PAR values were propagated to calculate the error in CbPM-NPP. The standard deviations of triplicate 24-hour $^{14}$C uptake incubations were propagated to calculate the error in $^{14}$C-NPP estimates.

For calculating error in NCP and net $C_{ph}$ accumulation, uncertainties in $dO_{2bio}/dt$, $dPOC/dt$ and $dC_{ph}/dt$ were equivalent to the confidence interval of the best-fit slope of linear regression of each variable against time. Standard deviations of averaged $\Delta O_2/Ar$, $k_{O2}$, $d[O_2]_{bio}/d[N_2O]_{bio}$ and $d[N_2O]_{bio}/dz$ values, and the mean relative errors of $k_{N2O}$, $[N_2O]_{meas}$, $[N_2O]_{Eq}$, and $[N_2O]_{thermal}$ reported in Izett et al. (2018), were propagated into errors for $NCP_{O2/Ar}$ and $NCP_{POC}$. Finally, to account for uncertainty in the photosynthetic quotient (PQ), we applied a PQ variability of 0.1 to drifter period 1 $NCP_{O2/Ar}$ calculations, following Laws (1991). We

https://doi.org/10.5194/bg-2019-257
Preprint. Discussion started: 8 July 2019


applied a higher PQ error of 0.3 to drifter period 2 calculations because the assumption of a PQ of 1.4 is more uncertain at this site, where regenerated production, associated with a lower PQ, is more likely.

## 3 Results

### 3.1 Water mass properties

Ship-board underway measurements revealed clear differences in hydrographic and biogeochemical characteristics between the water masses sampled by the two drifters. Surface water properties at drifter site 1 reflected the presence of a recently upwelled water mass that was relatively cold (11.8 ± 0.4 °C), saline (32.6 ± 0.04 g/kg), and nutrient-rich (Figs.1, S2, S3). The Pacific Fisheries Environmental Laboratory's coastal upwelling index at 45°N, 125°W exceeded 0 throughout drifter period 1. In contrast, the water mass tracked by the second drifter deployment was warmer (17.5 ± 0.1°C) and fresher (31.8 ± 0.05 g/kg), with lower average mixed layer nutrient concentrations.

Examination of surface water hydrographic properties during the two drifter deployments suggest that both drifters tracked a relatively homogenous water mass, excluding a period of increasing salinity during the first day of drifter deployment 1, and several transient temperature and salinity excursions after the second night of this deployment (grey patches in Fig. S2). These features indicate potential intrusion of an external water mass, possibly a result of loss of the drifter drogue (Sect. 2.1). Observations during these periods were thus screened out of the data set prior to analysis. Outside of these intervals, variability in salinity (drifter 1: 32.5–32.7 g/kg; drifter 2: 31.8–31.9 g/kg) was small during both drifter deployments. Variability in sea surface temperature was also limited (drifter 1: 11.2–13.0 °C, drifter 2: 17.3–17.7 °C), and largely reflected a diel cycle of warming and cooling, which was particularly evident for drifter period 2.

Temporal differences in CTD cast profiles point to some variation in mixed layer depth ($z_{mld}$) during both drifter deployments. In general, there were no multi-day trends in $z_{mld}$ through both periods, suggesting that transient shifts in water column turbulence likely contributed to changes in the shape of temperature, salinity, dissolved oxygen and fluorescence profiles. Average $z_{mld}$ values, calculated per drifter period, had relatively low relative standard deviations

https://doi.org/10.5194/bg-2019-257
Preprint. Discussion started: 8 July 2019


(<25%) and were applied to all subsequent calculations (Sect. 2.3). A sensitivity analysis, not shown, indicated that the choice of mixed layer depth using different criteria (i.e., fluorescence profiles, density profiles and the density difference criterion) and different time scales of integration (i.e., daytime/nighttime, 24 hour, and multi-day) did not significantly impact the results discussed below.

Average mixed layer nutrient concentrations fluctuated during both drifter deployments, but did not exhibit regular diurnal cycles (Fig. S3). At drifter site 1, concentrations ranged from 0.74 to 0.85 µM phosphate, 7.8 to 9.0 µM nitrate and nitrite, and 9.2 to 11.1 µM dissolved silica, excluding day 1 of the drifter deployment and anomalously high concentrations measured during a noisy CTD cast at midnight on the last day of the deployment. Excluding these outliers, a significant ($p<0.05$) linear regression of each nutrient concentration against time revealed that phosphate concentrations decreased by ~0.07 µM, [$NO_3^-$ + $NO_2^-$] decreased by 0.9 µM, and [$SiO_2$] decreased by 1.2 µM over the three-day drifter period. Nutrient concentrations varied less at site 2, from 0.08–0.10 µM [$PO_4^{3-}$], 0.29–0.61 µM [$NO_3^-$ + $NO_2^-$], and 1.2–1.7 [$SiO_2$]. While [$PO_4^{3-}$] and [$SiO_2$] increased significantly ($p<0.05$) by 0.015 µM and 0.48 µM, respectively, the change was small compared to the shift observed during drifter period 1.

### 3.2 Biogeochemical comparisons between drifter sites

Elevated nutrient concentrations at the drifter 1 site supported high productivity and the accumulation of phytoplankton biomass, as indicated by elevated chlorophyll-a ([Chl-a]= 0.66–1.5 µg/L), phytoplankton carbon ([$C_{ph}$]= 83–115 µg/L) and particulate organic carbon concentrations ([POC]= 130–261 µg/L) (Figs. 2a–c). We observed [$C_{ph}$]/[Chl-a] ratios ranging from 68–143 g/g, with a median value of 85 g/g (Fig. 2f). Using the carbon-based production model (CbPM; Sect. 2.5) and daily-averaged mixed layer PAR derived from satellite values matched to drifter location (within 5 km), these [$C_{ph}$]/[Chl-a] ratios translate into phytoplankton growth rates ranging from 0.75–0.94 $d^{-1}$. At the second drifter site, phytoplankton productivity and biomass were significantly lower in the nutrient-poor waters ([Chl-a]= 0.06–0.21 µg/L, [$C_{ph}$]= 11–17 µg/L, and [POC]= 25–38 µg/L). Ratios of [$C_{ph}$] to [Chl-a] at site 2 were significantly higher ($p<0.05$) than those observed at site 1, ranging from 69 g/g to 203 g/g, with a median value of 108 g/g. The higher ratios may reflect reduced cellular [Chl-a] associated with

https://doi.org/10.5194/bg-2019-257
Preprint. Discussion started: 8 July 2019


greater nutrient limitation, higher daily-integrated PAR, and proportionally more picoplankton than microplankton at drifter site 2 ( Westberry et al., 2008; Hirata et al., 2011; Graff et al., 2016; Burt et al., 2018). Median PAR levels were higher and less variable at this site, leading to lower variability in CbPM-based growth rates, which ranged from 0.81 to 0.85 $d^{-1}$.

Several lines of evidence suggest that the phytoplankton assemblage at drifter site 1 was enriched in large-celled phytoplankton, as compared to drifter site 2. The wavelength-dependent slope of particulate backscatter ($b_{bp}$) was lower at site 1 (range: 1.4 to 1.6, median: 1.5) than at site 2 (1.9–2.3, median = 2.1) (Fig. 2d), indicating proportionally larger particle sizes (Stramska et al., 2003; Kostadinov et al., 2009). This observation is supported by size-fractionated Chl-a measurements. During the drifter 1 deployment, the >20 µm size fraction (Sect. 2.4), increased from 21 % to 46 % of the total Chl-a pool, suggesting the enrichment of large phytoplankton in the assemblage. Indeed, pigment-based estimates of phytoplankton taxonomic composition and size class (Hirata et al., 2011; Zeng et al., 2018) suggested that relative diatom and microplankton abundances exceeded 50 % on the final sampling time point (Fig. 3e). By comparison, size-fractionated [Chl-a] and HPLC analyses from drifter 2 indicated a lower proportion of large-celled phytoplankton, with 9–15 % of total Chl in the >20 µm size fraction, and diatoms and micro-plankton comprising 19–29 % of the phytoplankton assemblage. The proportion of picoplankton increased through time at drifter site 2 from 31–50 % of total [Chl-a], alongside slight increase in $b_{bp}$ slope, indicating accumulation of smaller particle sizes (Fig. S2d). Finally, median bulk refractive index values across three wavelengths (470 nm, 532 nm, 650 nm) were higher at site 1 (1.08–1.11) than at site 2 (1.02–1.04) (Fig. S2e), which is consistent with a greater proportion of diatom-derived amorphous silica in the particle pool (Lide, 1997; Twardowski et al., 2001).

### 3.3 Diurnal variability and net community production

As shown in Fig. 3a, clear diurnal cycles in biological oxygen saturation ($\Delta O_2/Ar$) were observed during both drifter deployments. Slopes of linear regressions of $\Delta O_2/Ar$ against time were generally positive in the daytime, and negative at night (Fig. S4a). During drifter deployment 1, this diurnal cycle was superimposed on a longer-term increase in biological $O_2$ saturation as under-saturated values returned toward atmospheric equilibrium. At least part of

https://doi.org/10.5194/bg-2019-257
Preprint. Discussion started: 8 July 2019


this increase is attributable to gas exchange (optode-based measurements show increasing, but sub-saturated absolute $O_2$ concentrations during the entire drifter 1 period), which would act to erase $O_2$ under-saturation in the mixed layer caused by recent upwelling. However, calculation of the sea-air $O_2$ flux shows that, except for the first 24 hour period, only a small amount of the daily increase in $\Delta O_2/Ar$ can be explained by gas exchange ($J_{ex}$ < 10 mmol $O_2$ $m^{-2}$ $d^{-1}$). We thus attribute the temporal $\Delta O_2/Ar$ change to a primarily biological source. During drifter deployment 1, net community production calculated from $\Delta O_2/Ar$ diel cycles, corrected for gas exchange and vertical mixing ($NCP_{O2/Ar}$), was 165 mmol C-$m^{-2}$ $d^{-1}$ during the first 24 hours, decreasing to 104 mmol C-$m^{-2}$ $d^{-1}$ during the second day, and returning to 170 mmol C-$m^{-2}d^{-1}$ on the last day (Fig. 4).

Examination of the diel variability in POC, $C_{ph}$ and Chl-a revealed significant differences in the behavior of these variables as compared to $\Delta O_2/Ar$ (Fig. 3b–d). Whereas $\Delta O_2/Ar$ increased during the first drifter deployment, [POC] and [Chl-a] values decreased, and [$C_{ph}$] values remained relatively constant (Fig. 3b–d). Vertical mixing ($F_{mix,POC}$), accounted for 51 mmol $m^{-2}$ $d^{-1}$ of these daily changes in [POC]. Daily-integrated net community production (NCP) calculated using diel cycles in [POC] was positive (81 mmol C-$m^{-2}$ $d^{-1}$) during the first 24-hour period, negative (-14 mmol C $m^{-2}$ $d^{-1}$) during the second day, and positive again but much lower (6 mmol C $m^{-2}$ $d^{-1}$) during the third day.

Daily averaged net primary productivity (NPP), derived from the CbPM model (Sect. 2.5), declined from 147 mmol C $m^{-2}$ $d^{-1}$ on day 1 of drifter deployment 1 to 112 mmol C $m^{-2}$ $d^{-1}$ on day 3 (Table 1), reflecting the trend in Chl-a concentrations used to derive NPP (Fig. 3d). The CbPM-derived NPP estimate was similar to that obtained in $^{14}C$ incubations (150 ± 18 mmol C-$m^{-2}d^{-1}$) within the first 24 hours of drifter deployment 1. However, $^{14}C$-based NPP estimates on the third day of the deployment (49 ± 8 mmol C-$m^{-2}d^{-1}$) were about two-fold lower than those obtained from CbPM calculations.

Daily-integrated NCP was lower at drifter site 2, consistent with the lower observed phytoplankton biomass and nutrient concentrations. Compared to the drifter site 1, diel variability in $\Delta O_2/Ar$ and [POC] was more tightly coupled during the second drifter deployment, with closer agreement between the two measures of NCP (Fig 3). Both $O_2/Ar$ and [POC] displayed regular diel cycles, increasing in the daytime and decreasing at night (Fig. S4a–b). Over the full drifter deployment, concentrations of $C_{ph}$, Chl-a and, to a lesser extent, POC

https://doi.org/10.5194/bg-2019-257
Preprint. Discussion started: 8 July 2019


decreased, in contrast to $\Delta O_2/Ar$, which remained relatively constant across days. Values of $NCP_{O2/Ar}$ ranged from 20 to 26 mmol C $m^{-2}$ $d^{-1}$ over two consecutive 24 hour periods, while $NCP_{POC}$ values ranged from -3 to 1 mmol C $m^{-2}$ $d^{-1}$ (Fig. 4). NPP based on the CbPM calculations was 22 mmol C $m^{-2}$ $d^{-1}$ on the first day of the drifter period and 18 mmol C $m^{-2}$ $d^{-1}$ on the second day, while NPP calculated from one $^{14}C$ bottle incubation during the first day of the drifter 2 deployment was 12 ± 4 mmol C $m^{-2}$ $d^{-1}$, showing reasonably good agreement with values derived from the CbPM calculations (Table 1).

## 4 Discussion

The results from our Lagrangian surveys illustrate diurnal dynamics in two contrasting productivity regimes off the Oregon coast. Biogeochemical properties during the first drifter deployment suggested a dynamic, highly productive phytoplankton community, influenced by upwelling and elevated mixed layer nutrient concentrations (Figs. 1, S2). Several lines of evidence imply the presence of a developing diatom bloom at this site. Increasing mixed layer biological oxygen saturation ($\Delta O_2/Ar$) was contrasted by a general decrease in particulate organic carbon (POC) concentrations, suggesting a significant decoupling between $O_2$ and POC dynamics. In contrast, biogeochemical properties during the second drifter deployment were indicative of a lower productivity, nutrient-limited phytoplankton assemblage, with near-zero $\Delta O_2/Ar$ values reflecting a close balance between water column photosynthesis and respiration (Fig. 3a). Relative to the drifter 1 site, diel cycles in $\Delta O_2/Ar$ and POC were more closely coupled, while phytoplankton biomass ($C_{ph}$) and chlorophyll-a (Chl-a) concentrations (dominated by smaller cells) varied little through time. The contrasting properties between the two drifter deployments enable us to examine the coupling of $O_2$ and POC dynamics under different ecological states.

### 4.1 Decoupling of NCP and POC dynamics in the mixed layer

#### 4.1.1. Drifter 1

https://doi.org/10.5194/bg-2019-257
Preprint. Discussion started: 8 July 2019


In the absence of significant POC sinking and net loss to the dissolved organic carbon (DOC) pool, $NCP_{POC}$ should approximate $NCP_{O2/Ar}$ (Claustre et al., 2007; White et al., 2017). However, over the three successive 24-hour periods of drifter deployment 1, $NCP_{O2/Ar}$ values were consistently higher than $NCP_{POC}$, with the absolute difference increasing from 84 mmol C $m^{-2}$ $d^{-1}$ to 165 mmol C $m^{-2}$ $d^{-1}$ (Fig. 4). Moreover, net $C_{ph}$ accumulation, independently obtained from BB-3 measurements, were also consistently lower than $NCP_{O2/Ar}$, with offsets of 157 mmol C $m^{-2}$ $d^{-1}$ during the first 24-hour period, 83 mmol C $m^{-2}$ $d^{-1}$ during the second day, and 208 mmol C $m^{-2}$ $d^{-1}$ during the last day. Although some fraction of the $C_{ph}$ signal may be depressed as a result of vertical mixing (Sect. 2.6), this result suggests that much of the discrepancy between $NCP_{POC}$ and $NCP_{O2/Ar}$ may be attributed to $C_{ph}$ dynamics.

The increasingly negative $NCP_{POC}$ values over the course of the drifter 1 deployment primarily reflect diminishing rates of POC accumulation (dPOC/dt term in Eq. (8)) in the daytime (Fig. S4). This suggests that additional POC losses, including particle export and DOC accumulation, have decoupled $O_2$ from POC dynamics. During a diatom bloom, enhanced aggregation of large silica-rich particles and zooplankton fecal pellet production can stimulate export of POC and diatom cells out of the mixed layer, progressively decreasing $NCP_{POC}$ values relative to $NCP_{O2/Ar}$. A number of previous studies have reported enhanced particle fluxes associated with diatoms blooms in various oceanic regions (Buesseler, 1998; Guidi et al., 2009; Brzezinski et al., 2015; Stukel et al., 2017) . The global compilation of Henson et al. (2012) reported maximum export fluxes of ~83 mmol C $m^{-2}$ $d^{-1}$ from Southern Ocean measurements, while Alkire et al. (2012) observed maximum export fluxes of 96 mmol C $m^{-2}$ $d^{-1}$ during termination of the North Atlantic spring bloom. Stukel et al. (2017) applied the steady-state $^{234}Th$-$^{238}U$ approach to quantify export fluxes of ~36 mmol C $m^{-2}$ $d^{-1}$ in the nearshore region of the Southern California Current system. The upper values of these estimates are in the range of the discrepancy we measured between $NCP_{POC}$ and $NCP_{O2/Ar}$, suggesting that POC flux could potentially account for a significant fraction of the inferred POC loss at drifter site 1.

Additional constraints on POC fluxes can be derived from examining nutrient budgets. Over the three-day drifter deployment (Sect. 3.1), surface Si, N and P concentrations declined in a ratio of 17: 13: 1, which is consistent with the stoichiometry expected for organic matter produced by a diatom-rich assemblage (Brzezinski et al., 1998; Turner et al., 1998; Brzezinski, 2004). Assuming that the observed decrease in $SiO_2$ concentrations over the three days is

https://doi.org/10.5194/bg-2019-257
Preprint. Discussion started: 8 July 2019


attributable to export of diatomaceous particles out of the mixed layer, and applying a stoichiometric ratio of 106 C: 16 Si, we estimate an average carbon export value of ~50 mmol C $m^{-2}$ $d^{-1}$ and cumulative particle export flux of 150 mmol C $m^{-2}$ over the entire drifter period. This value is within a factor of two of the $NCP_{POC}$- $NCP_{O2/Ar}$ difference we observed, suggesting that POC export was a significant driver in decoupling POC and $\Delta O_2/Ar$.

Another likely POC loss is DOC production through cellular exudation, viral lysis and/or grazing (Briggs et al., 2018; Claustre et al., 2007; Dall'Olmo et al., 2011; Lochte et al., 1993). Loss of POC to the DOC pool would lower $NCP_{POC}$ and daily net $C_{ph}$ accumulation without affecting $NCP_{O2/Ar}$ values if the DOC produced is not respired in the mixed layer. While we did not conduct direct measurements of DOC concentrations during the cruise, previous work in a variety of ocean environments has shown that DOC production can account for 3-37% of NCP in the Ross Sea, up to 10-40% in the equatorial Pacific Ocean, and up to 66% in the Sargasso Sea during the seasonal bloom (Hansell and Carlson, 1998). More recently, Alkire et al. (2012) estimated that 22-40% of NCP was released into the DOC pool during the North Atlantic bloom. Taking an upper bound of 40% of NCP as DOC production yields a daily-integrated DOC flux of 41 to 68 mmol C $m^{-2}$ $d^{-1}$ (Fig. 4). The remaining discrepancy between $\Delta O_2/Ar$ and POC-based NCP estimates, 18 to 97 mmol C $m^{-2}$ $d^{-1}$ (average= 64 mmol C $m^{-2}$ $d^{-1}$), may be attributed to the export flux. These export values are consistent with the nutrient drawdown calculations above (50 mmol C $m^{-2}$ $d^{-1}$), and are sufficient to account for the NCP discrepancy.

A final consideration involves diurnal variation of zooplankton abundances and grazing rates, which may introduce an additional POC loss process decoupling mixed layer $POC/C_{ph}$ and dissolved $\Delta O_2$ dynamics ( Dall'Olmo et al., 2011; Briggs et al., 2018). During our expedition, we observed a strong signature of diel migrating zooplankton based on increased signal spikes in surface optical backscatter measurements during the night (Burt and Tortell, 2018). In addition to particle sinking and DOC excretion, these nighttime migrations could enhance POC and $C_{ph}$ loss at night without depleting $\Delta O_2/Ar$, if POC uptake rates exceed respiration rates. For example, (Wu et al., 2010) observed that mesozooplankton prefer to graze diatom-dominated assemblages at night over day in the East China Sea. Assuming that biomass accumulation rates from grazing surpasses grazer respiration rates (Dagg et al., 1982), these diurnal variations would contribute to more POC loss than $O_2$ loss. In addition, once POC is assimilated into the body of a grazer, it joins a larger particle size class that likely exceeds the size-dependent detection limits of the

https://doi.org/10.5194/bg-2019-257
Preprint. Discussion started: 8 July 2019


beam attenuation coefficient (Stramski and Kiefer, 1991; Marra, 2002; Claustre et al., 2007;), decreasing the $c_p$ signal used to derive POC.

**4.1.2 Drifter 2.** Compared to drifter site 1, absolute differences in $NCP_{O2/Ar}$ and $NCP_{POC}$ estimates were consistently smaller at drifter site 2, ranging from 23 to 25 mmol C $m^{-2}d^{-1}$ over two 24-hour periods (Fig. 4). Differences between $NCP_{O2/Ar}$ and net $C_{ph}$ accumulation were similar, ranging from 27–29 mmol C $m^{-2}d^{-1}$. This difference could be greater if we overestimated our assumption of a photosynthetic quotient of 1.4, which was based on new production rather than regenerated production (see error bars in Fig. 4). Nonetheless, the closer agreement across NCP estimates is consistent with the view of drifter site 2 as a more oligotrophic ecosystem, where primary production and heterotrophic consumption are more tightly coupled (Claustre et al., 2007; White et al., 2017). Such a coupling between phytoplankton production and loss through mortality and predation acts to dampen variability in phytoplankton biomass and NCP.

The smaller differences between $NCP_{O2/Ar}$ and $NCP_{POC}$ suggest a lower potential for POC sinking, DOC production and grazing to decouple POC, $C_{ph}$ and $\Delta O_2/Ar$ dynamics at drifter site 2. Lower 440 nm absorption values in the filtration blanks (Sect. 2.2) compared to drifter site 1 suggest lower colored dissolved organic matter (CDOM) concentrations at drifter site 2 (Organelli et al., 2014; Peacock et al., 2014). These observations are consistent with several previous observations of lower DOC production in lower productivity and/or oligotrophic waters (Bif et al., 2018; Hansell and Carlson, 1998). A recent compilation of summertime DOC production and NCP measurements along the Line P transect in the Northeast Pacific Ocean, shows that DOC production comprises at most 28% of total NCP in offshore waters (Bif and Hansell, 2019). Even if DOC/NCP ratios at drifter site 2 were as high as 28%, this would result in low overall DOC concentrations, because NCP rates are relatively low.

In addition, lower particle sinking rates are generally expected from phytoplankton assemblages dominated by small particle sizes <20µm, consistent with the higher $b_{bp}$ slope values and Chl-a size fractionation measurements at drifter site 2 (Sect. 3.2; Fig. 2) (Fowler and Knauer, 1986; Guidi et al., 2008). Nonetheless, these POC sinks, particularly export, are non-negligible for the low productivity system at drifter station 2, and could account for the entire discrepancy between measures of NCP. For example, an early JGOFS study reported that picoplankton comprised 70-90% of total carbon exported from the mixed layer in the equatorial

https://doi.org/10.5194/bg-2019-257
Preprint. Discussion started: 8 July 2019


Pacific Ocean and Arabian Sea (Richardson and Jackson, 2007). More recently, Durkin et al., (2015) reported significant rates of particle sinking from the small-celled, oligotrophic communities that dominate the BATS station. Finally, although organic matter recycling in smaller-celled communities is generally associated with tighter microbial loops, it is possible that grazing by zooplankton would also enhance loss of these phytoplankton cells from the mixed layer (Guidi et al., 2009). As we observed at drifter site 1, increased variability in the bbp signal suggest the presence of vertically migrating zooplankton into the mixed layer during nighttime intervals of drifter period 2 (Burt and Tortell, 2018).

### 4.2 Other factors driving variability in $NCP_{POC}$

In interpreting our results, it is important to consider a number of potential caveats, including methodological uncertainties and other POC sinks that could contribute to the variability in derived NCP estimates, POC export and DOC excretion rates. In our analysis, we interpret variations in particulate backscatter ($b_{bp}$) and beam attenuation ($c_p$) in terms of phytoplankton and total particulate organic carbon concentrations, assuming a small influence of inorganic suspended minerals from the continental shelf, Columbia River discharge or other sources. However, the Columbia River plume has been observed to extend south along the coast as far as ~44.5° N in the summertime (Thomas and Weatherbee, 2006), close to the location of drifter deployment 1. Moreover, the drifter was deployed ~40 km from shore over the continental shelf, where bottom resuspension of particles and their subsequent upwelling into the mixed layer is possible. Estimates of the bulk refractive index of particles ($\eta_p$), can be used to estimate the influence of inorganic minerals in our optical measurements. During drifter deployment 1, we observed median $\eta_p$ values at 470, 532 and 650 nm that were generally below 1.12 (Fig. S2e), whereas inorganic minerals in seawater, have a bulk refractive index as high as 1.26 (Lide, 1997; Twardowski et al., 2001). In addition, mixing with the fresh Columbia River plume would have significantly reduced salinity at drifter site 1 to values below 30 g/kg (Hickey et al., 1998), well below the 32 g/kg we observed during this drifter deployment (Sect. 3.1; Fig. S2c), which are consistent with salinities observed in the offshore Northeast Pacific Ocean (Whitney and Freeland, 1999). While these relatively high salinities support our assertion of a negligible influence of riverine particles on our measurements, the observed $\eta_p$ values do not preclude the

https://doi.org/10.5194/bg-2019-257
Preprint. Discussion started: 8 July 2019


presence of mixing between POC and a small fraction of shelf-derived inorganic particles at drifter site 1. By contrast, calculated $\eta_p$ values during deployment 2 were below 1.08, which is close to values expected for water-containing predominantly non-diatom phytoplankton organic carbon.

Additional uncertainty in our analysis derives from the algorithms used to estimate POC and phytoplankton carbon $C_{ph}$ from optical measurements (Sect. 2.2). Because of particle size limitations in the optical measurements, variability in seawater optical properties may not fully capture all significant components of the particulate pool, such as larger microplankton and zooplankton. Indeed, larger zooplankton often appear as erratic signal spikes in backscatter data (Burt and Tortell, 2018), which are typically filtered out during data processing. Moreover, the $c_p$ signal at 660 nm, used to derive [POC], responds most strongly to particles within the 0.5–20 µm diameter range (Claustre et al., 2007; Marra, 2002; Stramski and Kiefer, 1991), which is smaller than many large diatoms, fecal pellets and particle aggregates. This size bias would cause an underestimate of larger particles, and therefore [POC], measured by beam attenuation, thereby contributing to the apparent discrepancy between diel changes in [POC] and diel changes in $\Delta O_2/Ar$ (Fig. 4). Despite these potential caveats, recent work ( Graff et al., 2016; Briggs et al., 2018; Burt et al., 2018) has demonstrated that $c_p$ and $b_{bp}$-based derivations of [POC] and [$C_{ph}$] can indeed be robust in high biomass ocean regions, where productivity and the proportion of large-celled phytoplankton may be greater.

Changes in the $c_p$-to-[POC] relationship through time could also drive apparent variability in our optical [POC] estimates during both drifter deployments. On a global scale, the linear regression of [POC] against $c_p$ at 660 nm measured in samples from diverse marine environments is defined over a range of POC concentrations from ~5 to ~175 µg/L (Graff et al. 2015). At drifter site 2, the POC concentrations fell within the range of this fit. The assumption of a constant POC/$c_{p660}$ ratio close to the value suggested by Graff et al. (2015), is less likely to impact the derivation of apparent POC standing stocks and associated NCP estimates. Based on relatively small changes in $b_{bp}$ slope values (Figs. S2d, S4e) and phytoplankton community composition (Fig. 3e), it is unlikely that changes in particle size and bulk refractive index would have significantly shifted the relationship between POC and $c_{p660}$ during drifter deployment 2.

As concentrations of POC at drifter station 1 were 25% higher than the empirical limits of the $c_p$-based algorithm in (Graff et al., 2015), a different POC/$c_p$ relationship (i.e., different

https://doi.org/10.5194/bg-2019-257
Preprint. Discussion started: 8 July 2019


slope of the linear fit) could apply. In a limited comparison with discrete POC samples, we found a POC–$c_p$ slope that was similar to that of Graff et al. (albeit with a different y intercept) (Fig. S1). Nonetheless, we cannot rule out changes in the $c_{p660}$–[POC] relationship due to shifts in cell size and, to a lesser extent, bulk refractive index resulting from diatom accumulation (Kheireddine and Antoine, 2014; Stramski and Reynolds, 1993) (Figs. 3e, S2d–e). Indeed, Briggs et al. (2018) observed that the ratio of [POC] to $c_p$ decreased by ~20% during the rise of the North Atlantic bloom, while values increased by ~60% during the bloom decline. If we assume a 20% decrease in POC/$c_{p660}$ values (from ~420 to ~340 mg $m^{-2}$) associated with diatom growth (Briggs et al., 2018), our daily $NCP_{POC}$ estimates would be closer to 0, less positive during day 1 and less negative during days 2–3. This, in turn, would increase the apparent decoupling between $NCP_{POC}$ and $NCP_{O2/Ar}$ on day 1, and bring the values slightly closer on days 2–3. The value of these potential changes is small (<11%) relative to the differences we observed between $NCP_{O2/Ar}$ and $NCP_{POC}$. We thus conclude that variable POC/$c_{p660}$ ratios cannot explain the observed decoupling between POC, $C_{ph}$ and dissolved $O_2$ dynamics at the drifter 1 site.

### 4.3 Reconciling NCP and NPP

During both drifter surveys, we estimated daily-integrated net primary productivity (NPP) values using carbon-based productivity model (CbPM) calculations and $^{14}C$ bottle incubations (Sect. 2.5). On several days, these two measures of NPP estimates were consistently lower than $NCP_{O2/Ar}$ integrated over the same time scales and mixed layer depths (Table 1; Fig. 4). In theory, this result is impossible, as NCP includes additional respiration terms not included in NPP, and must always be equal to or (more realistically) lower than NPP. Recent work in the Northeast Pacific Ocean, has reported mean NCP/NPP ratios of 0.16 and 0.26 for offshore and coastal waters, respectively (Burt et al., 2018), based on $\Delta O_2$/Ar measurements and CbPM calculations. These ratios were determined from continuous observations along a ship-track, and not based on the analysis of diel cycles, as reported here. Similar to our observations, Briggs et al. (2018) and Alkire et al. (2012) also reported NCP values that were equal to or greater than NPP values obtained from different methodologies during their Lagrangian study of the North Atlantic Bloom.

https://doi.org/10.5194/bg-2019-257
Preprint. Discussion started: 8 July 2019


We observed a particularly large difference between $^{14}$C-NPP and $NCP_{O2/Ar}$ during the last day of drifter survey 1 (Table 1). It is unlikely that this difference is caused by changing environmental conditions, like PAR or cloudiness. During the three days of drifter survey 1, daily-integrated shipboard surface PAR observations changed by less than 15% day to day. Similarly, satellite-derived daily surface PAR shifted by at most 12%. More likely, methodological effects depressed $^{14}$C-NPP relative to both CbPM-NPP and $NCP_{O2/Ar}$. One possibility, which has been discussed at length by various authors (Gieskes et al., 1979; Fogg and Calvario-Martinez, 1989; Marra, 2009), is that bottle containment effects limit accurate estimates of $^{14}$C uptake. This likely caused underestimates of $^{14}$C-NPP during both drifter surveys, relative to CbPM-NPP and $NCP_{O2/Ar}$. In addition, during this last $^{14}$C-uptake experiment of drifter survey 2, incubator temperatures changed significantly, which could significantly impact phytoplankton growth rates during the incubation and result in depressed $^{14}$C-NPP values (Eppley, 1968).

A number of factors may also depress CbPM-based NPP estimates. While the model applies a satellite-based relationship between [Chl-a]/[$C_{ph}$] and daily mixed layer irradiance ($E_g$) to calculate growth rate, these $E_g$ values may not fully parametrize phytoplankton physiology for mixed assemblages in the ocean (Westberry et al., 2008). Indeed, phytoplankton photophysiology varies with other environmental conditions and phytoplankton composition (Cloern et al., 1995; Geider et al., 1998; MacIntyre et al., 2002; Westberry et al., 2008). In addition, the CbPM does not allow calculated growth rates to exceed 2 $d^{-1}$, which may not apply to all ocean environments (Graff et al., 2016). These uncertainties could potentially impact the applicability of the CbPM parameters to the specific ocean conditions at drifter sites 1 and 2.

### 4.4 Comparison to other studies

A number of previous studies have examined diurnal variation in upper ocean phytoplankton and organic particle dynamics across a variety of productivity regimes, from oligotrophic environments (Claustre et al., 1999, 2007; Wu et al., 2010; Gernez et al., 2011; Kheireddine and Antoine, 2014; Thyssen et al., 2014; Nicholson et al., 2015; Ribalet et al., 2015; White et al., 2017), to higher productivity waters and phytoplankton blooms (Brunet and Lizon, 2003; Wu et al., 2010; Alkire et al., 2012; Gernez et al., 2011; Dugenne et al., 2014; Kheireddine and Antoine, 2014; Needham and Fuhrman, 2016; Briggs et al., 2018). In general, these studies

https://doi.org/10.5194/bg-2019-257
Preprint. Discussion started: 8 July 2019


723 have shown that higher productivity environments exhibit higher amplitude diel cycles in beam
724 attenuation, POC concentration, phytoplankton cell abundances, Chl-a, and productivity,
725 consistent with the differences we observed between the distinct trophic environments of drifter
726 sites 1 and 2 (Figs. 2; S4).
727 To our knowledge, however, only two previous studies have directly compared diel
728 cycles in $O_2$-based and $c_p$-based mixed layer productivity using Lagrangian drifters (Alkire et al.,
729 2012; Briggs et al., 2018). This previous work demonstrated that NCP dynamics derived from
730 dissolved $O_2$ measurements differed from net POC accumulation over the course of the North
731 Atlantic bloom, with the magnitude of this disparity varying as a function of bloom stage. The
732 authors found that highest rates of POC export and DOC production, corresponding to the
733 greatest $O_2$-POC discrepancy, occurred during the main period of the bloom development, prior
734 to its termination. The results of our study off the Oregon coast extend these previous
735 observations from the North Atlantic bloom into two new surface ocean regimes: a high
736 productivity Pacific upwelling zone, and lower productivity offshore region. The upwelling
737 environment was characterized by rapid diatom accumulation, yielding significant differences
738 between $NCP_{O2/Ar}$ and $NCP_{POC}$ and net $C_{ph}$ accumulation, as observed at the height of the N.
739 Atlantic bloom. In contrast, the low productivity site exhibited tighter coupling between POC
740 and $O_2$ dynamics, and daily-integrated measures of NCP and net carbon accumulation. This
741 result supports the use of diurnal measurements of beam attenuation to estimate $NCP_{POC}$ in low
742 productivity regimes where POC and $O_2$/Ar dynamics are generally coupled. However, in higher
743 productivity regions, including coastal upwelling zones, additional measurements are likely
744 required to constrain the organic carbon mass balance. Such coupled measurements offer the
745 opportunity to simultaneously estimate surface water $O_2$ accumulation, net DOC production and
746 vertical transport of deep water to the mixed layer at high temporal resolution.
747
748 **5 Conclusions**
749
750 In the current study, biological oxygen saturation ($\Delta O_2$/Ar) and optically-derived
751 particulate organic carbon (POC) were measured continuously and simultaneously during two
752 Lagrangian drifter deployments. This dual measurement approach allowed us to examine the
753 (de)coupling between carbon and dissolved oxygen in surface waters, and facilitated direct

https://doi.org/10.5194/bg-2019-257
Preprint. Discussion started: 8 July 2019


754 comparison of $O_2$/Ar and POC-derived measures of net community production (NCP). Further,
755 the deployment of the drifters in contrasting hydrographic regimes allowed us to assess and
756 compare the diel cycles of $O_2$ and POC across a productivity gradient, from a mesotrophic
757 upwelling-influenced system, to an oligotrophic system further off shore. The results suggest that
758 $O_2$ and POC-based measures of NCP diverge in mid-to-high productivity phytoplankton
759 communities, where daily fluctuations in $\Delta O_2$/Ar are decoupled from POC cycling. In contrast,
760 the two NCP estimates showed better agreement in lower productivity regions, where $O_2$ and
761 POC cycles appeared to be more tightly coupled.
762 The disparity between POC and $O_2$-based NCP estimates offers an opportunity to
763 continuously track POC fate in the mixed layer using autonomous ship-board or in situ sensors.
764 As it is difficult and labor intensive to measure POC export on short time scales with sediment
765 traps and the $^{234}$Th-$^{238}$U disequilibrium method (Buesseler et al., 2006; Savoye et al., 2006),
766 simultaneous underway measurements of dissolved $O_2$, particulate beam attenuation and CDOM
767 absorption may provide a valuable, first-order approximation of POC partitioning among living
768 phytoplankton biomass, particle export and dissolved organic carbon (DOC) in the surface ocean
769 on short time scales. For studies in upwelling regions, it is further important to account for
770 entrainment of deep seawater in the mixed layer, and its effect on not only $NCP_{O2/Ar}$ calculations
771 (Izett et al., 2018), but also on $NCP_{POC}$ estimates through dilution of the surface POC signature.
772 In future work, independent estimates of POC export during each drifter deployment, through
773 sediment traps or depth-resolved backscatter profiles (Briggs et al., 2013, 2018), could validate
774 estimates of POC export fluxes derived from coupled $O_2$ and POC dynamics. It is also valuable
775 to constrain particle size, and partitioning of POC into detrital and living (phytoplankton and
776 heterotrophic bacteria) components to properly assess the size range captured by optics-based
777 POC and $C_{ph}$ measurements. There is significant future potential to exploit coupled $O_2$ and $c_p$
778 measurements on a multitude of ocean moorings to resolve opportunistic, high-resolution POC
779 export time series (Stramska and Dickey, 1992; Kinkade et al., 1999; Dickey and Chang, 2002).
780 Examples include the Optical Dynamics Experiment (North Pacific), the Biowatt II program
781 (North Atlantic), and the Bermuda Testbed Mooring program (BATS), spanning a variety of
782 ocean environments from the Arabian Sea to the North Pacific Ocean. Deployment of such
783 autonomous measurement systems across a range of oceanic regions will help to constrain POC
784 and productivity dynamics on global scales.

https://doi.org/10.5194/bg-2019-257
Preprint. Discussion started: 8 July 2019


## Data availability

Discrete and underway optical measurements may be accessed at https://github.com/srosengard/rosengard-tortell-oc2017.git

## Author contributions

Sarah Rosengard, Philippe Tortell, and Nina Schuback collected the data in the field. Robert Izett processed the CTD cast data and nitrous oxide measurements. Sarah Rosengard wrote the manuscript with significant input from the co-authors.

## Competing interests

The authors declare that they have no conflict of interest.

## Acknowledgements

Special thanks to Jessie Gwinn, Jay Pinckney, Ross McCulloch, Chen Zeng, Melissa Beaulac, Chris Payne and Maureen Soon for assistance in field collection and analysis of samples. This project was funded by the Natural Sciences and Engineering Research Council of Canada (NSERC), and by the US National Science Foundation (NSF project number 1436344).

## References

Alkire, M. B., D'Asaro, E., Lee, C., Jane Perry, M., Gray, A., Cetinić, I., Briggs, N., Rehm, E., Kallin, E., Kaiser, J. and González-Posada, A.: Estimates of net community production and export using high-resolution, Lagrangian measurements of O2, NO3−, and POC through the evolution of a spring diatom bloom in the North Atlantic, Deep Sea Res. Part I Oceanogr. Res. Pap., 64, 157–174, doi:10.1016/j.dsr.2012.01.012, 2012.

Behrenfeld, M. J., Boss, E., Siegel, D. A. and Shea, D. M.: Carbon-based ocean productivity and

https://doi.org/10.5194/bg-2019-257
Preprint. Discussion started: 8 July 2019


816 phytoplankton physiology from space, Global Biogeochem. Cycles, 19(1), 2005.
817 Bif, M. B. and Hansell, D. A.: Seasonality of dissolved organic carbon in the upper Northeast
818 Pacific Ocean, Global Biogeochem. Cycles, 2019.
819 Bif, M. B., Hansell, D. A. and Popendorf, K. J.: Controls on the fate of dissolved organic carbon
820 under contrasting upwelling conditions, Front. Mar. Sci., 5, 463, 2018.
821 Boss, E., Twardowski, M. S. and Herring, S.: Shape of the particulate beam attenuation spectrum
822 and its inversion to obtain the shape of the particulate size distribution, Appl. Opt., 40(27), 4885–
823 4893, 2001.
824 de Boyer Montégut, C., Madec, G., Fischer, A. S., Lazar, A. and Iudicone, D.: Mixed layer depth
825 over the global ocean: An examination of profile data and a profile-based climatology, J.
826 Geophys. Res., 109(C12), C12003, doi:10.1029/2004JC002378, 2004.
827 Briggs, N., Guðmundsson, K., Cetinić, I., D'Asaro, E., Rehm, E., Lee, C. and Perry, M. J.: A
828 multi-method autonomous assessment of primary productivity and export efficiency in the
829 springtime North Atlantic, Biogeosciences, 15(14), 4515–4532, 2018.
830 Briggs, N. T., Slade, W. H., Boss, E. and Perry, M. J.: Method for estimating mean particle size
831 from high-frequency fluctuations in beam attenuation or scattering measurements, Appl. Opt.,
832 52(27), 6710–6725, 2013.
833 Brunet, C. and Lizon, F.: Tidal and diel periodicities of size-fractionated phytoplankton pigment
834 signatures at an offshore station in the southeastern English Channel, Estuar. Coast. Shelf Sci.,
835 56(3–4), 833–843, 2003.
836 Brzezinski, M., Villareal, T. and Lipschultz, F.: Silica production and the contribution of diatoms
837 to new and primary production in the central North Pacific, Mar. Ecol. Prog. Ser., 167, 89–104,
838 doi:10.3354/meps167089, 1998.
839 Brzezinski, M. A.: The Si:C:N ratio of marine diatoms: Interspecific variability and the effect of
840 some environmental variables, J. Phycol., 21(3), 347–357, doi:10.1111/j.0022-
841 3646.1985.00347.x, 2004.
842 Brzezinski, M. A., Krause, J. W., Bundy, R. M., Barbeau, K. A., Franks, P., Goericke, R.,
843 Landry, M. R. and Stukel, M. R.: Enhanced silica ballasting from iron stress sustains carbon
844 export in a frontal zone within the California Current, J. Geophys. Res. Ocean., 120(7), 4654–
845 4669, 2015.
846 Buesseler, K. O.: The decoupling of production and particulate export in the surface ocean,

https://doi.org/10.5194/bg-2019-257
Preprint. Discussion started: 8 July 2019




847 Global Biogeochem. Cycles, 12(2), 297–310, 1998.
848 Buesseler, K. O., Benitez-Nelson, C. R., Moran, S. B., Burd, A., Charette, M., Cochran, J. K.,
849 Coppola, L., Fisher, N. S., Fowler, S. W. and Gardner, W. D.: An assessment of particulate
850 organic carbon to thorium-234 ratios in the ocean and their impact on the application of 234Th as
851 a POC flux proxy, Mar. Chem., 100(3–4), 213–233, 2006.
852 Burt, W. J. and Tortell, P. D.: Observations of Zooplankton Diel Vertical Migration From High-
853 Resolution Surface Ocean Optical Measurements, Geophys. Res. Lett., 45(24), 13–396, 2018.
854 Burt, W. J., Westberry, T. K., Behrenfeld, M. J., Zeng, C., Izett, R. W. and Tortell, P. D.:
855 Carbon: Chlorophyll Ratios and Net Primary Productivity of Subarctic Pacific Surface Waters
856 Derived From Autonomous Shipboard Sensors, Global Biogeochem. Cycles, 32(2), 267–288,
857 doi:10.1002/2017GB005783, 2018.
858 Capelle, D. W., Dacey, J. W. and Tortell, P. D.: An automated, high through-put method for
859 accurate and precise measurements of dissolved nitrous-oxide and methane concentrations in
860 natural waters, Limnol. Oceanogr. Methods, 13(7), 345–355, 2015.
861 Cassar, N., Barnett, B. A., Bender, M. L., Kaiser, J., Hamme, R. C. and Tilbrook, B.: Continuous
862 high-frequency dissolved O2/Ar measurements by equilibrator inlet mass spectrometry, Anal.
863 Chem., 81(5), 1855–1864, 2009.
864 Cassar, N., Nevison, C. D. and Manizza, M.: Correcting oceanic O2/Ar-net community
865 production estimates for vertical mixing using N2O observations, Geophys. Res. Lett., 41(24),
866 8961–8970, 2014.
867 Claustre, H., Morel, A., Babin, M., Cailliau, C., Marie, D., Marty, J., Tailliez, D. and Vaulot, D.:
868 Variability in particle attenuation and chlorophyll fluorescence in the tropical Pacific: Scales,
869 patterns, and biogeochemical implications, J. Geophys. Res. Ocean., 104(C2), 3401–3422, 1999.
870 Claustre, H., Huot, Y., Obernosterer, I., Gentili, B., Tailliez, D. and Lewis, M.: Gross community
871 production and metabolic balance in the South Pacific Gyre, using a non intrusive bio-optical
872 method, Biogeosciences Discuss., 4(5), 3089–3121, 2007.
873 Cloern, J. E., Grenz, C. and Vidergar-Lucas, L.: An empirical model of the phytoplankton
874 chlorophyll: carbon ratio-the conversion factor between productivity and growth rate, Limnol.
875 Oceanogr., 40(7), 1313–1321, 1995.
876 Dagg, M. J., Vidal, J., Whitledge, T. E., Iverson, R. L. and Goering, J. J.: The feeding,
877 respiration, and excretion of zooplankton in the Bering Sea during a spring bloom, Deep Sea

https://doi.org/10.5194/bg-2019-257
Preprint. Discussion started: 8 July 2019




878 Res. Part A. Oceanogr. Res. Pap., 29(1), 45–63, 1982.
879 Dall'Olmo, G., Boss, E., Behrenfeld, M. J., Westberry, T. K., Courties, C., Prieur, L., Pujo-Pay,
880 M., Hardman-Mountford, N. and Moutin, T.: Inferring phytoplankton carbon and eco-
881 physiological rates from diel cycles of spectral particulate beam-attenuation coefficient,
882 Biogeosciences, 8(11), 3423–3439, 2011.
883 Dickey, T. D. and Chang, G. C.: Recent advances and future visions: temporal variability of
884 optical and bio-optical properties of the ocean, Oceanogr. DC-OCEANOGRAPHY Soc., 14(3),
885 15–29, 2002.
886 Dugenne, M., Thyssen, M., Nerini, D., Mante, C., Poggiale, J.-C., Garcia, N., Garcia, F. and
887 Grégori, G. J.: Consequence of a sudden wind event on the dynamics of a coastal phytoplankton
888 community: an insight into specific population growth rates using a single cell high frequency
889 approach, Front. Microbiol., 5, 485, 2014.
890 Durkin, C. A., Estapa, M. L. and Buesseler, K. O.: Observations of carbon export by small
891 sinking particles in the upper mesopelagic, Mar. Chem., 175, 72–81,
892 doi:10.1016/J.MARCHEM.2015.02.011, 2015.
893 Eppley, R. W.: An incubation method for estimating the carbon content of phytoplankton in
894 natural samples, Limnol. Oceanogr., 13(4), 574–582, doi:10.4319/lo.1968.13.4.0574, 1968.
895 Fogg, G. E. and Calvario-Martinez, O.: Effects of bottle size in determinations of primary
896 productivity by phytoplankton, Hydrobiologia, 173(2), 89–94, doi:10.1007/BF00015518, 1989.
897 Fowler, S. W. and Knauer, G. A.: Role of large particles in the transport of elements and organic
898 compounds through the oceanic water column, Prog. Oceanogr., 16(3), 147–194,
899 doi:10.1016/0079-6611(86)90032-7, 1986.
900 Garcia, H. E. and Gordon, L. I.: Oxygen solubility in seawater: Better fitting equations, Limnol.
901 Oceanogr., 37(6), 1307–1312, 1992.
902 Gardner, W. D., Walsh, I. D. and Richardson, M. J.: Biophysical forcing of particle production
903 and distribution during a spring bloom in the North Atlantic, Deep Sea Res. Part II Top. Stud.
904 Oceanogr., 40(1–2), 171–195, 1993.
905 Geider, R. J., Maclntyre, H. L. and Kana, T. M.: A dynamic regulatory model of phytoplanktonic
906 acclimation to light, nutrients, and temperature, Limnol. Oceanogr., 43(4), 679–694, 1998.
907 Gernez, P., Antoine, D. and Huot, Y.: Diel cycles of the particulate beam attenuation coefficient
908 under varying trophic conditions in the northwestern Mediterranean Sea: Observations and

https://doi.org/10.5194/bg-2019-257
Preprint. Discussion started: 8 July 2019


909 modeling, Limnol. Oceanogr., 56(1), 17–36, 2011.
910 Gieskes, W. W. C., Kraay, G. W. and Baars, M. A.: Current 14C methods for measuring primary
911 production: Gross underestimates in oceanic waters, Netherlands J. Sea Res., 13(1), 58–78,
912 doi:10.1016/0077-7579(79)90033-4, 1979.
913 Graff, J. R., Westberry, T. K., Milligan, A. J., Brown, M. B., Dall'Olmo, G., Dongen-Vogels, V.
914 van, Reifel, K. M. and Behrenfeld, M. J.: Analytical phytoplankton carbon measurements
915 spanning diverse ecosystems, Deep Sea Res. Part I Oceanogr. Res. Pap., 102, 16–25,
916 doi:10.1016/J.DSR.2015.04.006, 2015.
917 Graff, J. R., Westberry, T. K., Milligan, A. J., Brown, M. B., Olmo, G. D., Reifel, K. M. and
918 Behrenfeld, M. J.: Photoacclimation of natural phytoplankton communities, Mar. Ecol. Prog.
919 Ser., 542, 51–62, 2016.
920 Guidi, L., Jackson, G. A., Stemmann, L., Carlos Miquel, J., Picheral, M. and Gorsky, G.:
921 Author's personal copy Relationship between particle size distribution and flux in the
922 mesopelagic zone, , doi:10.1016/j.dsr.2008.05.014, 2008.
923 Guidi, L., Stemmann, L., Jackson, G. A., Ibanez, F., Claustre, H., Legendre, L., Picheral, M. and
924 Gorskya, G.: Effects of phytoplankton community on production, size, and export of large
925 aggregates: A world-ocean analysis, Limnol. Oceanogr., 54(6), 1951–1963, 2009.
926 Hamme, R. C., Cassar, N., Lance, V. P., Vaillancourt, R. D., Bender, M. L., Strutton, P. G.,
927 Moore, T. S., DeGrandpre, M. D., Sabine, C. L. and Ho, D. T.: Dissolved O2/Ar and other
928 methods reveal rapid changes in productivity during a Lagrangian experiment in the Southern
929 Ocean, J. Geophys. Res. Ocean., 117(C4), 2012.
930 Hansell, D. A. and Carlson, C. A.: Net community production of dissolved organic carbon,
931 Global Biogeochem. Cycles, 12(3), 443–453, 1998.
932 Henson, S. A., Sanders, R. and Madsen, E.: Global patterns in efficiency of particulate organic
933 carbon export and transfer to the deep ocean, Global Biogeochem. Cycles, 26(1), 2012.
934 Hickey, B. M., Pietrafesa, L. J., Jay, D. A. and Boicourt, W. C.: The Columbia River plume
935 study: Subtidal variability in the velocity and salinity fields, J. Geophys. Res. Ocean., 103(C5),
936 10339–10368, 1998.
937 Hirata, T., Hardman-Mountford, N. J., Brewin, R. J. W., Aiken, J., Barlow, R., Suzuki, K., Isada,
938 T., Howell, E., Hashioka, T. and Noguchi-Aita, M.: Synoptic relationships between surface
939 Chlorophyll-a and diagnostic pigments specific to phytoplankton functional types,

https://doi.org/10.5194/bg-2019-257
Preprint. Discussion started: 8 July 2019


940 Biogeosciences, 8(2), 311–327, 2011.
941 Hoppe, C. J. M., Schuback, N., Semeniuk, D. M., Maldonado, M. T. and Rost, B.: Functional
942 Redundancy Facilitates Resilience of Subarctic Phytoplankton Assemblages toward Ocean
943 Acidification and High Irradiance , Front. Mar. Sci. , 4, 229 [online] Available from:
944 https://www.frontiersin.org/article/10.3389/fmars.2017.00229, 2017.
945 Izett, R. W., Manning, C. C., Hamme, R. C. and Tortell, P. D.: Refined estimates of net
946 community production in the Subarctic Northeast Pacific derived from ΔO2/Ar measurements
947 with N2O-based corrections for vertical mixing, Global Biogeochem. Cycles, 32(3), 326–350,
948 2018.
949 Jin, X., Najjar, R. G., Louanchi, F. and Doney, S. C.: A modeling study of the seasonal oxygen
950 budget of the global ocean, J. Geophys. Res. Ocean., 112(C5), 2007.
951 Kaiser, J., Reuer, M. K., Barnett, B. and Bender, M. L.: Marine productivity estimates from
952 continuous O2/Ar ratio measurements by membrane inlet mass spectrometry, Geophys. Res.
953 Lett., 32(19), 2005.
954 Keeling, R. F. and Shertz, S. R.: Seasonal and interannual variations in atmospheric oxygen and
955 implications for the global carbon cycle, Nature, 358(6389), 723, 1992.
956 Kheireddine, M. and Antoine, D.: Diel variability of the beam attenuation and backscattering
957 coefficients in the northwestern Mediterranean Sea (BOUSSOLE site), J. Geophys. Res. Ocean.,
958 119(8), 5465–5482, 2014.
959 Kinkade, C. S., Marra, J., Dickey, T. D., Langdon, C., Sigurdson, D. E. and Weller, R.: Diel bio-
960 optical variability observed from moored sensors in the Arabian Sea, Deep sea Res. Part II Top.
961 Stud. Oceanogr., 46(8–9), 1813–1831, 1999.
962 Kostadinov, T. S., Siegel, D. A. and Maritorena, S.: Retrieval of the particle size distribution
963 from satellite ocean color observations, J. Geophys. Res., 114(C9), C09015,
964 doi:10.1029/2009JC005303, 2009.
965 Laws, E. A.: Photosynthetic quotients, new production and net community production in the
966 open ocean, Deep Sea Res. Part A. Oceanogr. Res. Pap., 38(1), 143–167, 1991.
967 Lide, D. R.: Physical and optical properties of minerals, CRC Handb. Chem. Phys., 4–130, 1997.
968 Lochte, K., Ducklow, H. W., Fasham, M. J. R. and Stienen, C.: Plankton succession and carbon
969 cycling at 47 N 20 W during the JGOFS North Atlantic Bloom Experiment, Deep Sea Res. Part
970 II Top. Stud. Oceanogr., 40(1–2), 91–114, 1993.

https://doi.org/10.5194/bg-2019-257
Preprint. Discussion started: 8 July 2019


971 Loisel, H., Nicolas, J.-M., Sciandra, A., Stramski, D. and Poteau, A.: Spectral dependency of
972 optical backscattering by marine particles from satellite remote sensing of the global ocean, J.
973 Geophys. Res., 111(C9), C09024, doi:10.1029/2005JC003367, 2006.
974 MacIntyre, H. L., Kana, T. M., Anning, T. and Geider, R. J.: Photoacclimation of irradiance
975 response curves and photosynthetic pigments in microalgae and cyanobacteria, J. Phycol., 38(1),
976 17–38, doi:10.1046/j.1529-8817.2002.00094.x, 2002.
977 Manning, C. C., Stanley, R. H. R., Nicholson, D. P., Smith, J. M., Pennington, J. T., Fewings, M.
978 R., Squibb, M. E. and Chavez, F. P.: Impact of recently upwelled water on productivity
979 investigated using in situ and incubation-based methods in Monterey Bay, J. Geophys. Res.
980 Ocean., 122(3), 1901–1926, 2017.
981 Marra, J.: Approaches to the measurement of plankton production, Phytoplankt. Product. Carbon
982 Assim. Mar. Freshw. Ecosyst., 78–108, 2002.
983 Marra, J.: Net and gross productivity: weighing in with 14C, Aquat. Microb. Ecol., 56(2–3),
984 123–131, doi:10.3354/ame01306, 2009.
985 Morel, A., Huot, Y., Gentili, B., Werdell, P. J., Hooker, S. B. and Franz, B. A.: Examining the
986 consistency of products derived from various ocean color sensors in open ocean (Case 1) waters
987 in the perspective of a multi-sensor approach, Remote Sens. Environ., 111(1), 69–88, 2007.
988 Murphy, J. and Riley, J. P.: A modified single solution method for the determination of
989 phosphate in natural waters, Anal. Chim. Acta, 27, 31–36, 1962.
990 Needham, D. M. and Fuhrman, J. A.: Pronounced daily succession of phytoplankton, archaea
991 and bacteria following a spring bloom, Nat. Microbiol., 1(4), 16005, 2016.
992 Nicholson, D. P., Wilson, S. T., Doney, S. C. and Karl, D. M.: Quantifying subtropical North
993 Pacific gyre mixed layer primary productivity from Seaglider observations of diel oxygen cycles,
994 Geophys. Res. Lett., 42(10), 4032–4039, 2015.
995 Organelli, E., Bricaud, A., Antoine, D. and Matsuoka, A.: Seasonal dynamics of light absorption
996 by chromophoric dissolved organic matter (CDOM) in the NW Mediterranean Sea (BOUSSOLE
997 site), Deep Sea Res. Part I Oceanogr. Res. Pap., 91, 72–85, 2014.
998 Peacock, M., Evans, C. D., Fenner, N., Freeman, C., Gough, R., Jones, T. G. and Lebron, I.: UV-
999 visible absorbance spectroscopy as a proxy for peatland dissolved organic carbon (DOC)
1000 quantity and quality: considerations on wavelength and absorbance degradation, Environ. Sci.
1001 Process. Impacts, 16(6), 1445–1461, 2014.

https://doi.org/10.5194/bg-2019-257
Preprint. Discussion started: 8 July 2019


1002 Raymond, P. A., Zappa, C. J., Butman, D., Bott, T. L., Potter, J., Mulholland, P., Laursen, A. E.,
1003 McDowell, W. H. and Newbold, D.: Scaling the gas transfer velocity and hydraulic geometry in
1004 streams and small rivers, Limnol. Oceanogr. Fluids Environ., 2(1), 41–53, 2012.
1005 Reuer, M. K., Barnett, B. A., Bender, M. L., Falkowski, P. G. and Hendricks, M. B.: New
1006 estimates of Southern Ocean biological production rates from O2/Ar ratios and the triple isotope
1007 composition of O2, Deep Sea Res. Part I Oceanogr. Res. Pap., 54(6), 951–974, 2007.
1008 Ribalet, F., Swalwell, J., Clayton, S., Jiménez, V., Sudek, S., Lin, Y., Johnson, Z. I., Worden, A.
1009 Z. and Armbrust, E. V.: Light-driven synchrony of Prochlorococcus growth and mortality in the
1010 subtropical Pacific gyre, Proc. Natl. Acad. Sci., 112(26), 8008–8012, 2015.
1011 Richardson, T. L. and Jackson, G. A.: Small phytoplankton and carbon export from the surface
1012 ocean., Science, 315(5813), 838–40, doi:10.1126/science.1133471, 2007.
1013 Riley, J. P.: Grasshoff, K. [Ed.] 1976. Methods of seawater analysis. Verlag Chemie, Weinheim
1014 and New York, xv+ 317 p. $43.60., 1977.
1015 Roesler, C. S. and Barnard, A. H.: Optical proxy for phytoplankton biomass in the absence of
1016 photophysiology: Rethinking the absorption line height, Methods Oceanogr., 7, 79–94, 2013.
1017 Savoye, N., Benitez-Nelson, C., Burd, A. B., Cochran, J. K., Charette, M., Buesseler, K. O.,
1018 Jackson, G. A., Roy-Barman, M., Schmidt, S. and Elskens, M.: 234Th sorption and export
1019 models in the water column: a review, Mar. Chem., 100(3–4), 234–249, 2006.
1020 Schuback, N., Flecken, M., Maldonado, M. T. and Tortell, P. D.: Diurnal variation in the
1021 coupling of photosynthetic electron transport and carbon fixation in iron-limited phytoplankton
1022 in the NE subarctic Pacific, Biogeosciences, 13, 1019–1035, doi:10.5194/bg-13-1019-2016,
1023 2016.
1024 Siegel, D. A., Dickey, T. D., Washburn, L., Hamilton, M. K. and Mitchell, B. G.: Optical
1025 determination of particulate abundance and production variations in the oligotrophic ocean, Deep
1026 Sea Res. Part A. Oceanogr. Res. Pap., 36(2), 211–222, 1989.
1027 Stanley, R. H. R., Kirkpatrick, J. B., Cassar, N., Barnett, B. A. and Bender, M. L.: Net
1028 community production and gross primary production rates in the western equatorial Pacific,
1029 Global Biogeochem. Cycles, 24(4), 2010.
1030 Stramska, M. and Dickey, T. D.: Short-term variations of the bio-optical properties of the ocean
1031 in response to cloud-induced irradiance fluctuations, J. Geophys. Res. Ocean., 97(C4), 5713–
1032 5721, 1992.


1033 Stramska, M. and Dickey, T. D.: Modeling phytoplankton dynamics in the northeast Atlantic
1034 during the initiation of the spring bloom, J. Geophys. Res. Ocean., 99(C5), 10241–10253, 1994.
1035 Stramska, M., Stramski, D., Hapter, R., Kaczmarek, S. and Ston´, J. S.: Bio-optical relationships
1036 and ocean color algorithms for the north polar region of the Atlantic, J. Geophys. Res, 108(C5),
1037 3143, doi:10.1029/2001JC001195, 2003.
1038 Stramski, D. and Kiefer, D. A.: Light scattering by microorganisms in the open ocean, Prog.
1039 Oceanogr., 28(4), 343–383, doi:10.1016/0079-6611(91)90032-H, 1991.
1040 Stramski, D. and Reynolds, R. A.: Diel variations in the optical properties of a marine diatom,
1041 Limnol. Oceanogr., 38(7), 1347–1364, 1993.
1042 Stukel, M. R., Aluwihare, L. I., Barbeau, K. A., Chekalyuk, A. M., Goericke, R., Miller, A. J.,
1043 Ohman, M. D., Ruacho, A., Song, H. and Stephens, B. M.: Mesoscale ocean fronts enhance
1044 carbon export due to gravitational sinking and subduction, Proc. Natl. Acad. Sci., 114(6), 1252–
1045 1257, 2017.
1046 Sullivan, J. M., Twardowski, M. S., Donaghay, P. L. and Freeman, S. A.: Use of optical
1047 scattering to discriminate particle types in coastal waters, Appl. Opt., 44(9), 1667,
1048 doi:10.1364/AO.44.001667, 2005.
1049 Thomas, A. C. and Weatherbee, R. A.: Satellite-measured temporal variability of the Columbia
1050 River plume, Remote Sens. Environ., 100(2), 167–178, doi:10.1016/J.RSE.2005.10.018, 2006.
1051 Thomson, R. E., Fine, I. V., Thomson, R. E. and Fine, I. V.: Estimating Mixed Layer Depth from
1052 Oceanic Profile Data, J. Atmos. Ocean. Technol., 20(2), 319–329, doi:10.1175/1520-
1053 0426(2003)020<0319:EMLDFO>2.0.CO;2, 2003.
1054 Thyssen, M., Grégori, G. J., Grisoni, J.-M., Pedrotti, M. L., Mousseau, L., Artigas, L. F., Marro,
1055 S., Garcia, N., Passafiume, O. and Denis, M. J.: Onset of the spring bloom in the northwestern
1056 Mediterranean Sea: influence of environmental pulse events on the in situ hourly-scale dynamics
1057 of the phytoplankton community structure, Front. Microbiol., 5, 387, 2014.
1058 Tortell, P. D.: Dissolved gas measurements in oceanic waters made by membrane inlet mass
1059 spectrometry, Limnol. Oceanogr. Methods, 3(1), 24–37, 2005.
1060 Tortell, P. D., Guéguen, C., Long, M. C., Payne, C. D., Lee, P. and DiTullio, G. R.: Spatial
1061 variability and temporal dynamics of surface water pCO2, ΔO2/Ar and dimethylsulfide in the
1062 Ross Sea, Antarctica, Deep Sea Res. Part I Oceanogr. Res. Pap., 58(3), 241–259, 2011.
1063 Tortell, P. D., Asher, E. C., Ducklow, H. W., Goldman, J. A. L., Dacey, J. W. H., Grzymski, J.


1064 J., Young, J. N., Kranz, S. A., Bernard, K. S. and Morel, F. M. M.: Metabolic balance of coastal
1065 Antarctic waters revealed by autonomous pCO2 and ΔO2/Ar measurements, Geophys. Res.
1066 Lett., 41(19), 6803–6810, 2014.
1067 Turner, R. E., Qureshi, N., Rabalais, N. N., Dortch, Q., Justic, D., Shaw, R. F. and Cope, J.:
1068 Fluctuating silicate: nitrate ratios and coastal plankton food webs, Proc. Natl. Acad. Sci., 95(22),
1069 13048–13051, 1998.
1070 Twardowski, M. S., Boss, E., Macdonald, J. B., Pegau, W. S., Barnard, A. H. and Zaneveld, J. R.
1071 V.: A model for estimating bulk refractive index from the optical backscattering ratio and the
1072 implications for understanding particle composition in case I and case II waters, J. Geophys. Res.
1073 Ocean., 106(C7), 14129–14142, doi:10.1029/2000JC000404, 2001.
1074 Wanninkhof, R.: Relationship between wind speed and gas exchange over the ocean revisited,
1075 Limnol. Oceanogr. Methods, 12(6), 351–362, 2014.
1076 Weiss, R. F. and Price, B. A.: Nitrous oxide solubility in water and seawater, Mar. Chem., 8(4),
1077 347–359, 1980.
1078 Westberry, T., Behrenfeld, M. J., Siegel, D. A. and Boss, E.: Carbon-based primary productivity
1079 modeling with vertically resolved photoacclimation, Global Biogeochem. Cycles, 22(2), 2008.
1080 White, A. E., Barone, B., Letelier, R. M. and Karl, D. M.: Productivity diagnosed from the diel
1081 cycle of particulate carbon in the North Pacific Subtropical Gyre, Geophys. Res. Lett., 44(8),
1082 3752–3760, 2017.
1083 Whitney, F. . and Freeland, H. .: Variability in upper-ocean water properties in the NE Pacific
1084 Ocean, Deep Sea Res. Part II Top. Stud. Oceanogr., 46(11–12), 2351–2370, doi:10.1016/S0967-
1085 0645(99)00067-3, 1999.
1086 Wu, C.-J., Chiang, K.-P. and Liu, H.: Diel feeding pattern and prey selection of
1087 mesozooplankton on microplankton community, J. Exp. Mar. Bio. Ecol., 390(2), 134–142, 2010.
1088 Zeng, C., Rosengard, S. Z., Burt, W., Peña, M. A., Nemcek, N., Zeng, T., Arrigo, K. R. and
1089 Tortell, P. D.: Optically-derived estimates of phytoplankton size class and taxonomic group
1090 biomass in the Eastern Subarctic Pacific Ocean, Deep Sea Res. Part I Oceanogr. Res. Pap., 136,
1091 107–118, 2018.
1092

https://doi.org/10.5194/bg-2019-257
Preprint. Discussion started: 8 July 2019




**Table 1**: Daily-integrated mixed layer net primary production (NPP) and net community production (NCP). All units are in mmol C $m^{-2}$ $d^{-1}$. Note that CbPM is the carbon-based productivity model (Sect. 2.5).

| | **Day #** | **NPP (CbPM)** | **NPP ($^{14}$C)** | **$NCP_{O2/Ar}$** |
|---|---|---|---|---|
| Drifter 1 | 1 | 147 ± 61 | 150 ±18 | 166 ± 49 |
| | 2 | 137 ± 51 | | 104 ± 29 |
| | 3 | 112 ± 40 | 49 ± 8 | 170 ± 36 |
| Drifter 2 | 1 | 22 ± 9 | 12 ± 4 | 20 ± 15 |
| | 2 | 18 ± 7 | | 26 ± 16 |

https://doi.org/10.5194/bg-2019-257
Preprint. Discussion started: 8 July 2019


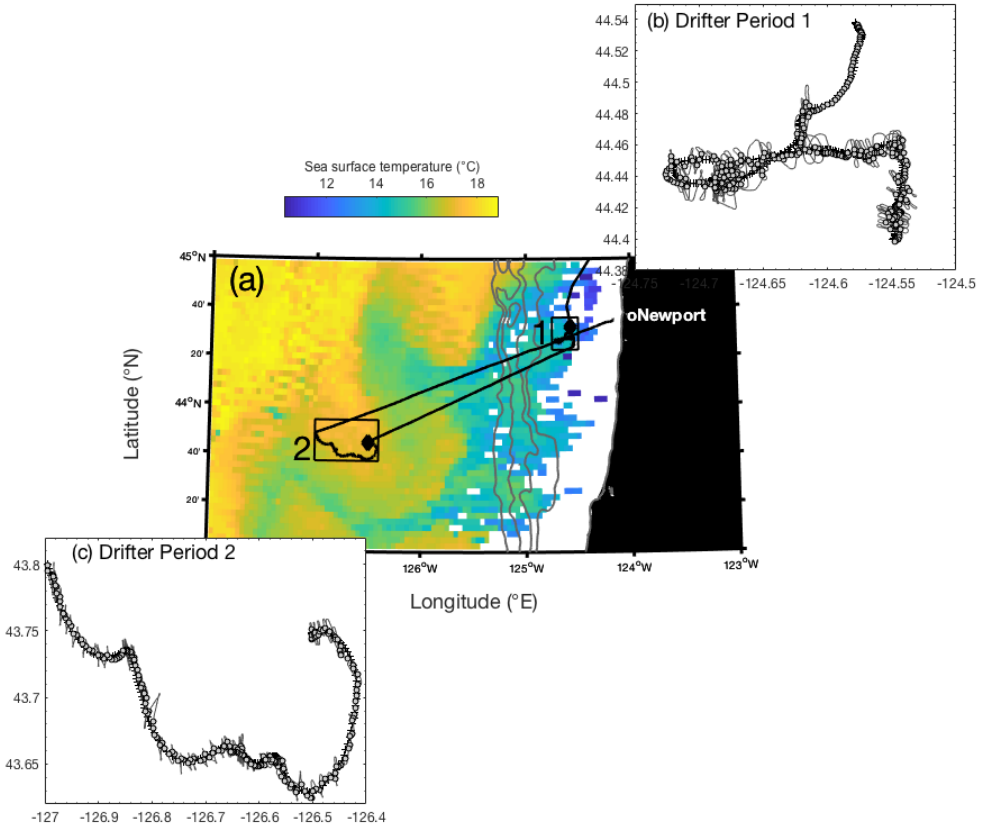


**Figure 1**: (a) Map of AQUA MODIS-derived 8-day composite sea surface temperature (11µm, nighttime) from 21-28 August 2017, overlapping with the duration of both drifter deployments. The two hollow boxes on the map denote location of drifter tracks, with the "x's" indicating the location of the initial release. Gray bathymetry contours extend from 0-2000 m, with deepest contours representing the extent of the continental shelf. Panels (b and c) show a detailed view of the two drifter tracks, with the ship's track shown in a light grey line and circles denoting times when the ship was <1.5 km away from the drifter position. Only measurements taken at these cross-over locations were used for analysis.

https://doi.org/10.5194/bg-2019-257
Preprint. Discussion started: 8 July 2019


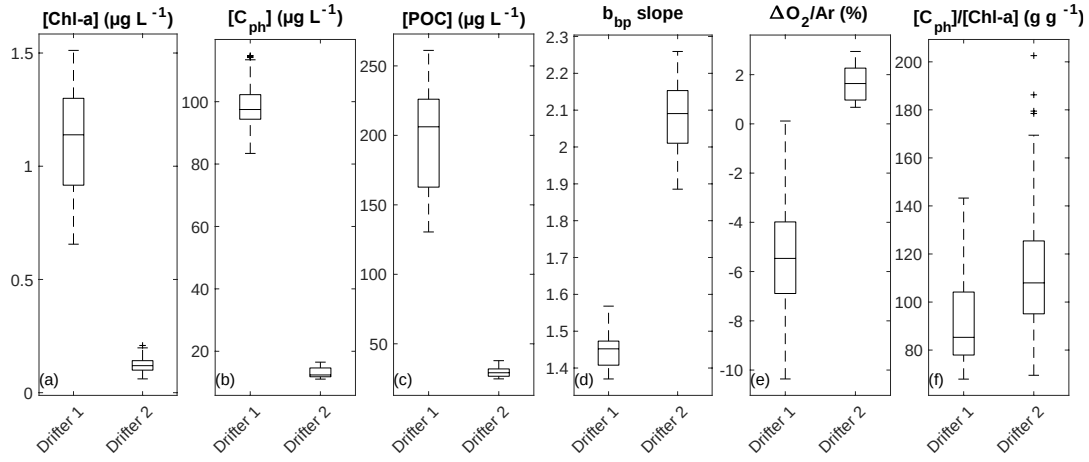


**Figure 2:** Comparison of average surface water properties between the two drifter deployments: (a) chlorophyll-a concentration (Chl-a), (b) phytoplankton carbon concentration ($C_{ph}$), (c) particulate organic carbon (POC) concentration, (d) the wavelength-dependent slope of particulate backscatter ($b_{bp}$), (e) biological oxygen saturation anomaly ($\Delta O_2/Ar$), and (f) the $[C_{ph}]$/[Chl-a] ratio. Boxes represent the median (center line) and 25 and 75 percentiles (box edges). Outliers are indicated as black "+" marks.

https://doi.org/10.5194/bg-2019-257
Preprint. Discussion started: 8 July 2019


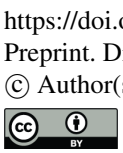

Biogeosciences
Discussions
Open Access
EGU

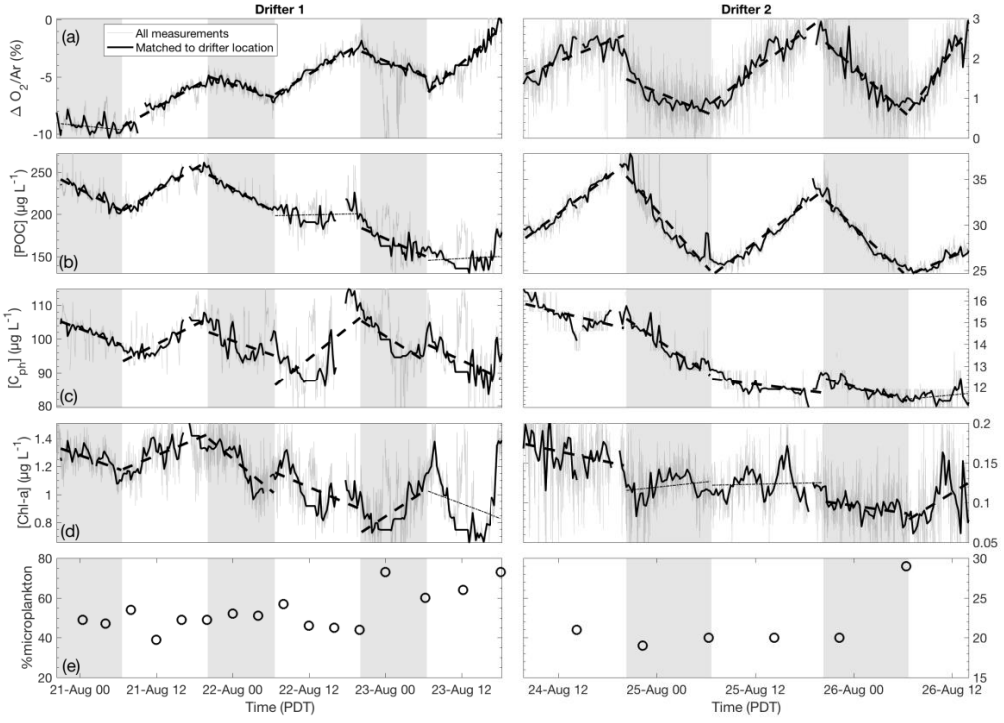


**Figure 3**: Time-series of (a) biological oxygen saturation ($\Delta O_2/Ar$), (b) particulate organic carbon (POC) concentration, (c) phytoplankton carbon ($C_{ph}$) concentration, (d) chlorophyll-a (Chl-a) concentration and (e) HPLC-derived microplankton relative abundances (%) during the two drifter deployments (left and right panels, respectively). For each daytime (non-shaded) and nighttime (shaded) interval, the best fit linear regression line is plotted. Significant regressions ($p<0.05$) are plotted as thick dashed lines, while non-significant regressions ($p\geq0.05$) are plotted as thin dotted lines. Grey lines show all measurements while thicker black line shows observations collected when the ship was within 1.5 km of the drifter location.

https://doi.org/10.5194/bg-2019-257
Preprint. Discussion started: 8 July 2019




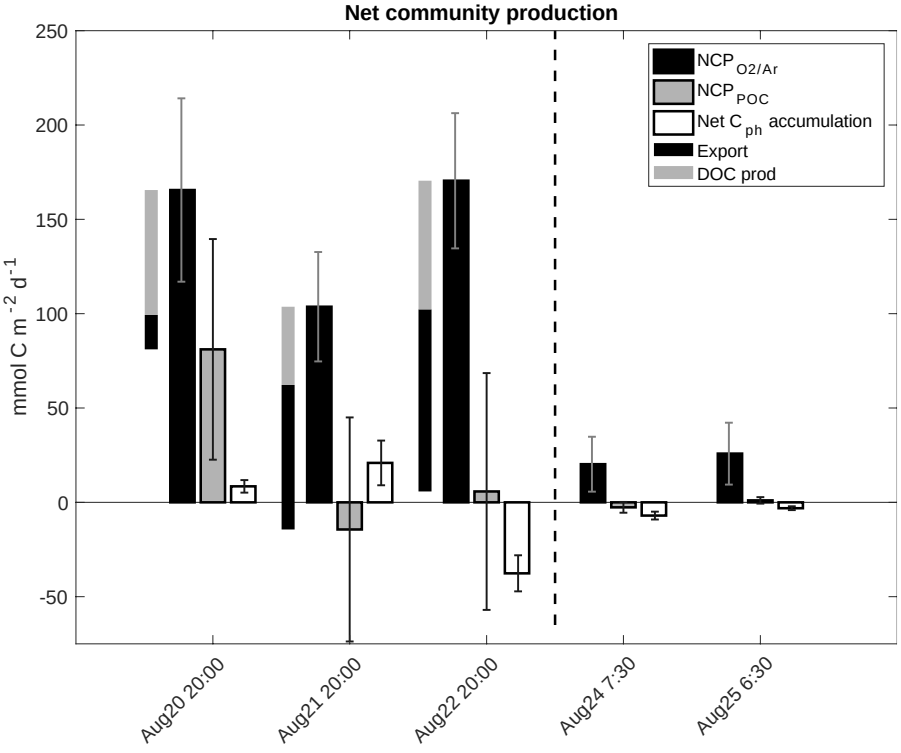


**Figure 4**: (Left axis) Daily net community production (NCP) and net phytoplankton carbon accumulation during successive days of the two drifter deployments derived from diel cycles of biological oxygen saturation ($\Delta O_2/Ar$), and particulate organic carbon (POC) concentration. Each set of thicker bars is for one 24-hour period, with approximate starting times on the x-axis. For drifter period 1, POC loss by particle export and DOC production sum up to the difference between $NCP_{O2/Ar}$ and $NCP_{POC}$.